Organic Dye-Sensitized Zirconium Doped CeO$_2$ Nanoparticles: Synthesis, Characterization andApplication in DSSCs

By

Syeda Hafsa Bukhari

Department of Chemistry

Quaid-I-Azam University,

Islamabad

2023

Organic Dye-Sensitized Zirconium Doped CeO$_2$ Nanoparticles: Synthesis, Characterization andApplication in DSSCs

A dissertation submitted to the Department of Chemistry, Quaid-I-Azam University, Islamabad, in partial fulfillment ofthe requirement for the degree of

Master of Philosophy

In

Physical Chemistry

By

Syeda Hafsa Bukhari

Department of Chemistry

Quaid-I-Azam University,

Islamabad

2023

بسم الله الرحمن الرحيم

This is to certify that this dissertation entitled **"Organic Dy-Sensitized Zirconium Doped CeO₂** *Nanoparticles: Synthesis Characterization and Application in DSSCs"* submitted by *Ms. Syeda Hafsa Bukhari*, is accepted in its present form by the Department of Chemistry, Quaid-i-Azam University, Islamabad, as satisfying the dissertation requirements for the degree of *Master of Philosophy in Physical Chemistry.*
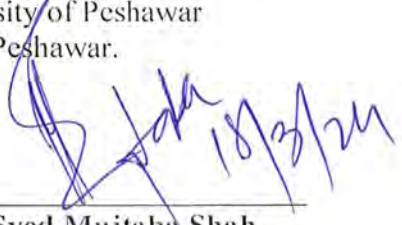
External Examiner:

Dr. Anwar ul Haq Ali Shah
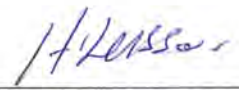Institute of Chemical Sciences
University of Peshawar
Peshawar.

Supervisor:

Prof. Dr. Syed Mujtaba Shah
Department of Chemistry
Quaid-i-Azam University
Islamabad

Head of Section:

Prof. Dr. Hazrat Hussain
Department of Chemistry
Quaid-i-Azam University
Islamabad

Chairman:

Prof. Dr. Aamer Saeed Bhatti (TI)
Department of Chemistry
Quaid-i-Azam University
Islamabad

DEDICATED TO MY PARENTS

for all their sacrifices, encouragement, and moral support whichpreceded this journey.

Acknowledgment

Prayers be to Allah Almighty for showering His blessings on me throughout my research work and for His ultimate guidance.

I would like to acknowledge my deep and warm thanks to my supervisor **Prof. Dr. Syed Mujtaba Shah**, Department of Chemistry, Quaid-i-Azam University, Islamabad, for giving me the opportunity to work under his supervision. His knowledge, motivation and sincerity to his profession has deeply inspired me and it is his guidance that carried me through all the stages of my research work. I am very fortunate to perform my research under his supervision. I pay my special regards to the Chairman of the Chemistry Department **Prof. Dr. Amir Saeed Bhatti** and the Head of Physical Section **Prof. Dr. Hazrat Hussain** for providing necessary academic and research facilities.

I am extremely grateful to my parents and siblings for their unconditional love, support, and valuable prayers. Specials thanks to them for believing in me and giving me this learning opportunity. I am also thankful to all teaching and non- teaching staff members of the department for their cooperative behavior during my research work.

I want to thank my friend **Arooj Fatima** for continuously supporting and motivating me throughout my work. I would extent my gratitude to my seniors especially **Syed Naimat Ullah** and **Mohammad Nasir Hussain** for always giving me better ideas to carry out the research and encouraging me during my work. I am grateful to my lab fellows and class fellows for keeping a friendly environment and helping me in my work.

I would also appreciate my friends for giving me great company and support. May Allah Almighty shower his limitless blessings and prosperity to all those who helped me in anyway during the completion of my thesis.

Syeda Hafsa Bukhari

Table of Contents

List of Figures

List of Tables

LIST OF ABBREVIATIONS

AZ	Arsenazo III
CA	Carminic Acid
CM	Centimeter
DSSCs	Dye Sensitized Solar Cells
EV	Electron Volt
FF	Fill Factor
FT-IR	Fourier Transform Infrared Radiation
FTO	Fluorine doped Tin Oxide
FWHM	Full Width at Half Maximum
HOMO	Highest Occupied Molecular Orbital
ITO	Indium doped Tin Oxide
J_{sc}	Short Circuit Current
LUMO	Lowest Unoccupied Molecular Orbital
mg	Milligram
mL	Milliliter
mM	Millimolar
M_{PP}	Maximum Power Point
nm	Nanometer
NPs	Nanoparticles
P3HT	Poly(3,4-hexylthiophene)
PEDOT:PSS	Poly(3,4-ethylenedioxythiophene)-poly(styrenesul fonate)
V_{oc}	Open Circuit Voltage
XRD	X-Ray Diffraction

ABSTRACT

In the present research work, pristine CeO_2 and (1-6)% transition metal (Zr) doped CeO_2 nanoparticles were successfully synthesized by co-precipitation method and characterized with UV-Visible spectroscopy, X-Ray powder diffraction (XRD), and Fourier transform infrared spectroscopy (FT-IR). UV-Visible spectroscopy was performed to investigate optical properties. It indicated that with an increase in Zirconium percentage ranging from 1 to 5%, a red shift was observed and with further increase indopant percentage, a decrease in wavelength was observed. Tauc plots of the synthesized nanoparticles showed tuning in band gap ranging from 3.25 to 2.65 eV. XRD analysis showed that the average crystallite size decreases with increasingdopant percentage. FR-IR was done to study functional group detection which confirmed that the prepared samples were pure and showed vibration bands of required samples. The nanoparticles were then used for the fabrication of nanohybrid assembly. FT-IR and UV-Visible spectra nanomaterial confirmed the successful sensitization of nanoparticles with CA and AZ dye. Nanohybrid materials were used as a photoanode in dye-sensitized solar cells (DSSCs). CA and AZ dyes were used as photosensitizers and P3HT used as a solid-state electrolyte to overcome drawbacks offered by liquid electrolyte. The nanohybrid materials showed a significant red shift towards the visible region with improved optical properties and better power conversion efficiency of DSSCs.

Chapter 1 Introduction

1.1 Energy Crisis

A nation's economy is reliant on its country's energy resources. We need energy to run electrical appliances in our homes, in factories and industries to manufacture various materials and other chemical products, in agriculture for mechanization, water pumping, and aggregation, and in almost every other area of ourlives. This energy is obtained by burning fossil fuels, and the world has been mainly dependent on them. Oil, natural gas, and coal are examples of fossil fuels. These non-renewable resources are formed from the remains of plants and animals over the course of hundreds of years underground. In addition to not being renewable, they significantly contribute to global warming and pollute our environment[1].

With the increasing population and modernization energy demands are increasing and world now needs to shift from non-renewable to inexhaustible energy resources for the production of electricity and fulfilling other energy demands the Figure 1.1 shows the non-renewable and renewable resources[2].
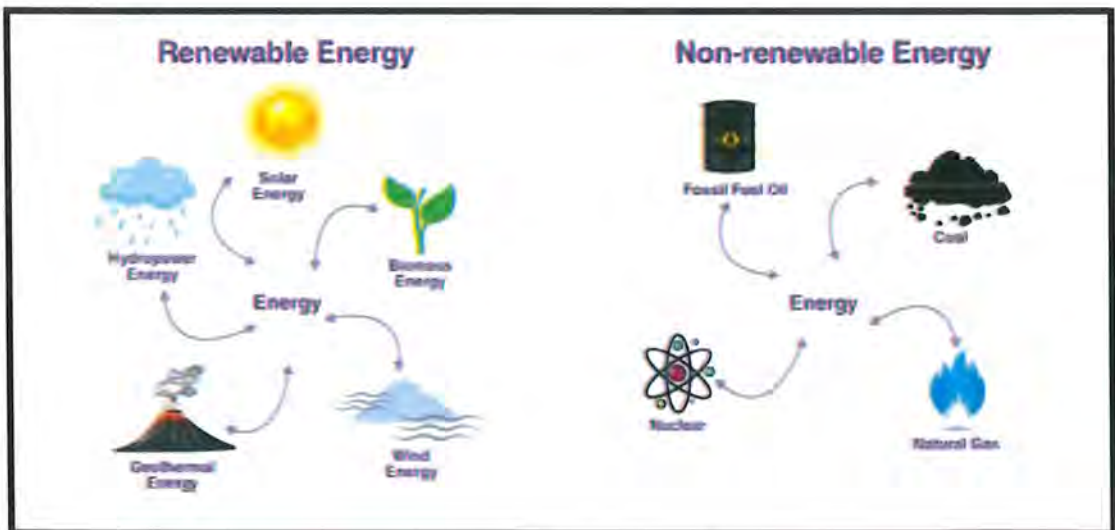
Figure. 1.1. Renewable and non-renewable energy resources[3].

Existing energy demands can be enhanced by utilizing natural resources such as sun, wind, water, and biomass. Figure 1.1 shows the variety of renewable and non-renewable resources. Sun is the ultimate source of energy.

Solar cells convert solar energy into other useful form of energy such as electricityto run the electrical appliances.

There are many varieties of devices working on the same principle but due to low efficiency and high cost they are not being widely used. Silicon is the most common semiconducting material having the high efficiency, but it is costly[5]. Solar cells combine to form solar panels, and many solar panels arranged in a proper way is termed as solar array. Solar energy converters are enlisted below which convert solar energy into useful form[6].
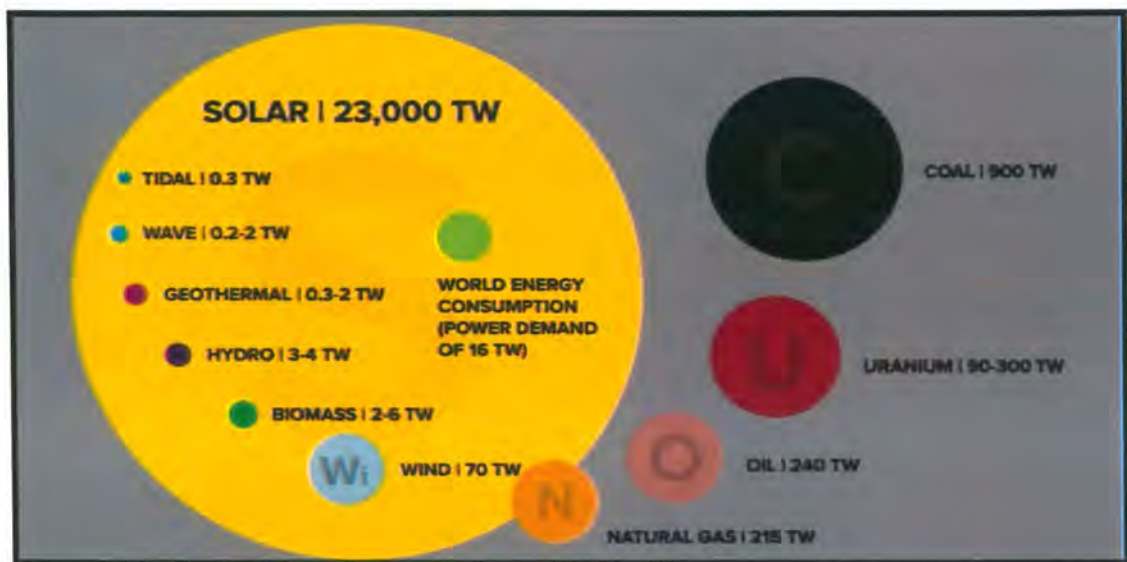
Figure. 1.2. Energy availability of different resources per year[7].

1.2 Solar Energy Converters

Solar energy converters are the technologies which are used to transform sunlight into other useful forms to fulfill growing population demands. It includes:

❖ Photovoltaic Converters
❖ Solar Thermal Converters
❖ Photochemical Converters

1.2.1 Photovoltaic Converters

Photovoltaic converters work on the principle of Photoelectric effect in semiconductors to convert the light radiation into electrical energy. There are two necessary steps to carry out this process.

i. Solar cell should absorb incoming light radiations and then convert this into chemical energy. As light falls on the cell, the electrons absorb this energy andget excited. After excitation they jump into higher energy levels temporarily storing the chemical energy. These excited electrons serve as charge carriers.

ii. Solar cells should exhibit resistance to prevent the dropping of the carriers back into ground level. Thus, potential difference is developed which is responsible to drive the electrons into the external circuit. Hence, electrical work is done.

Gap between valence band and conduction band is band gap. This gap is responsible for providing high energy levels to the excited electron for greater time than its relaxation time so the electrons can conduct electricity.

1.2.2 Solar Thermal Converters

These converters receive radiations and then convert this solar energy in the form of internal energy of the materials which results in increase in temperature of the cell. Due to this cell acts like a heat engine. For example, solar energy can be used to heat water and convert it into steam and then this steam can be used to drive the steam turbines and generate electricity[8].

1.2.3 Photochemical Energy Converters

The major difference between photochemical energy converters and photovoltaic energy converters is the conversion of energy in the form of permanent increase in chemical potential in case of the photochemical energy converters.

1.3 Semiconducting Materials

Band gap of semiconducting material is of two types:

i. **Direct Band Gap**

The lowest energy state in the conduction band and the highest energy state in the valence band lies at the same value of momentum[9].

ii. **Indirect Band Gap**

In indirect band gap, the highest energy of valence band and the lowest energy of conduction band does not occur at the same value of momentum and is illustrated in Figure 1.3.
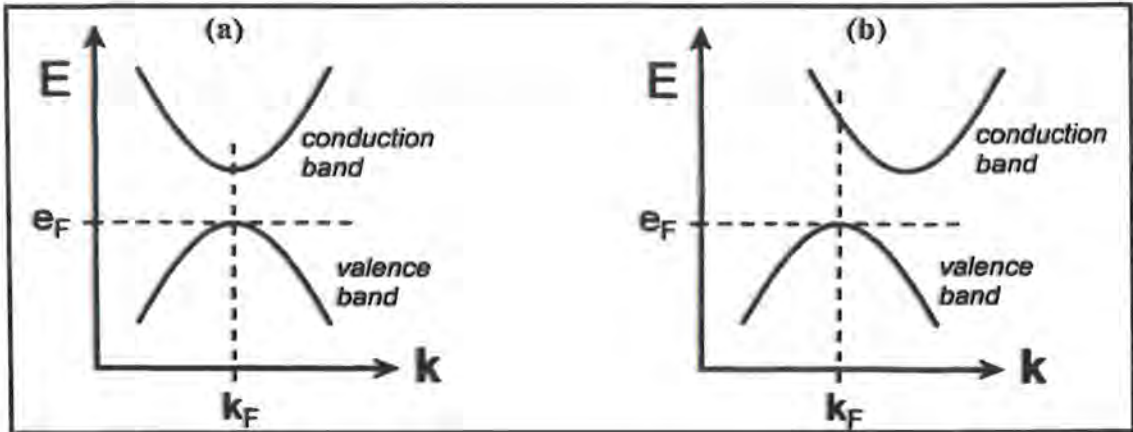
Figure. 1.3. Band gaps of semiconducting materials (a) direct band gap (b) indirect bandgap[10].

1.4 Solar Cell

A solar cell, also known as a photovoltaic (PV) cell, is a semiconductor device that converts sunlight into electricity through the photovoltaic effect. The direct conversion of solar energy into electricity is a clean and renewable energy source, commonly used in solar panels to harness the power of the sun for various applications, including residential and commercial electricity generation, as well as off-grid and remote power supply systems. Solarcells play a crucial role in the transition to sustainable and environmentally friendly energy sources, decreasing dependence on fossil fuels and justifying climate change.

1.4.1 Working of a Photovoltaic Cell

Solar cell work on the principle of photovoltaic effect which involves the direct conversion of solar energy into electricity on the absorption of light by a semiconducting material. These devices are typically constructed from semiconductor materials like silicon. When sunlight strikes the solar cell, it causes the movement of electron within the material. This movement of electrons creates an electric current, which can be harnessed and used as electricity. The key to the efficiency of solar cells lies in the p-n junction within the semiconductor, where one side is positively doped (p-type) and the other is negativelydoped (n-type). This junction creates an electric field that drives the separated charge carriers (electrons and holes) towards opposite sides, thus generating a flow of electrons and creating electrical potential. By connecting an external circuit to the solar cell, the generated current can be captured and used to power electrical devices or stored in batteries for later use[11].

4

Figure 1.4. illustrates the generation of electric current from solar energy using a solar cell.
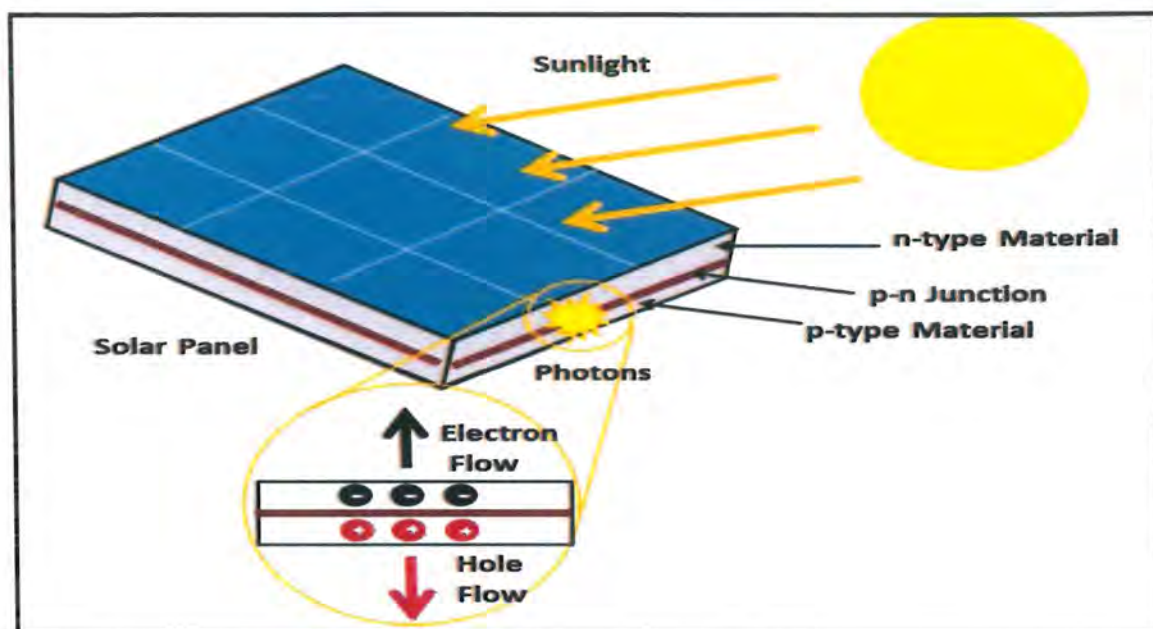
Figure. 1.4. Generation of charge carriers on the absorption of light by semiconductingmaterials[12].

1.4.2 Organic Solar Cells

When sunlight falls on surface of solar cell, electron hole pairs are generated. Then this electron hole pair splits up into free charge carries. This whole process take place at the donor acceptor interface or at the surface of photoactive material. After the separation of electron and hole from the pair, they move towards their corresponding electrodes and this type of separation of charge is usually carried out in organic solar cells.

1.4.3 Inorganic Solar Cells

Besides, when light hits the surface of inorganic solar cells, electron from lower states of energy gets excited to higher energy states that is conduction band, leaving a hole in the valence band increasing the population of electron in the conduction band which act as charge carriers. Inorganic solar cells work on this principle and produce useful energy (in form of photocurrent).

1.4.4   Charge Recombination

The separated charge carriers are involved in the production of photocurrent but the process of excitation is also opposed by the process of recombination of charge carriers resulting in decreasing the numbers of free charge carries and hence less photocurrent. Process of recombination is of different types these are:

I.   Radiative Recombination

As the names shows involves the emission of radiation accompanying the transfer of electron from conduction band back to the valance band and filling up the space created as a result of photoexcitation.

II.   Auger Recombination

It involves the inter transfer of energy between the charge carriers. Theelectron falling back to the valance band instead of giving off energy ofabsorption in form of photon transfer this energy to the other charge carries in the conduction band inform of kinetic energy[13].

III.   Non-Radiative Recombination

Because of presence of impurities and some crystal defects in lattice electrons instead of giving off photons in the process of recombination they emit the phonons also this process is accompanied with some lattice vibrations[14].
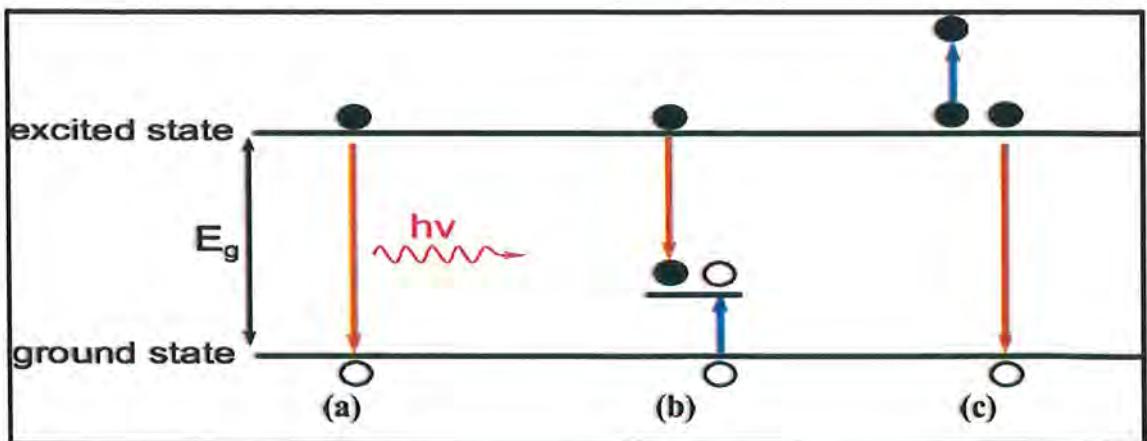
Figure. 1.5. Charge recombination (a) radiative recombination (b) non-radiativerecombination (c) auger recombination[13].

1.5 Generations of Solar Cells

Solar cells are classified into different generations these are:

1.5.1   First Generation Solar Cells

These are inorganic solar cells. These are the oldest type of solar cells, and it includes the monocrystalline silicon solar cells, polycrystalline silicon solar cells and amorphous silicon based solar cells they differ because of their fabrication. silicon and germanium are the efficient semiconducting materials for the solar cells but their high cost and in effectivity at the higher temperatures make them less attractive economically.

1.5.2 Second Generation Solar Cells

From first generation researchers had to move towards second generation where mainly organic material based solar cells were produced than that of inorganic material based first generation solar cells, because of the low cost and requirement of less temperature but they have less efficiency which made them less attractive.

1.5.3 Third Generation Solar Cells

This generation was fabricated for getting high efficiency and involving low-cost materials for their fabrication. Our interest is on the dye-sensitized solar cells (DSSCs) from this generation.
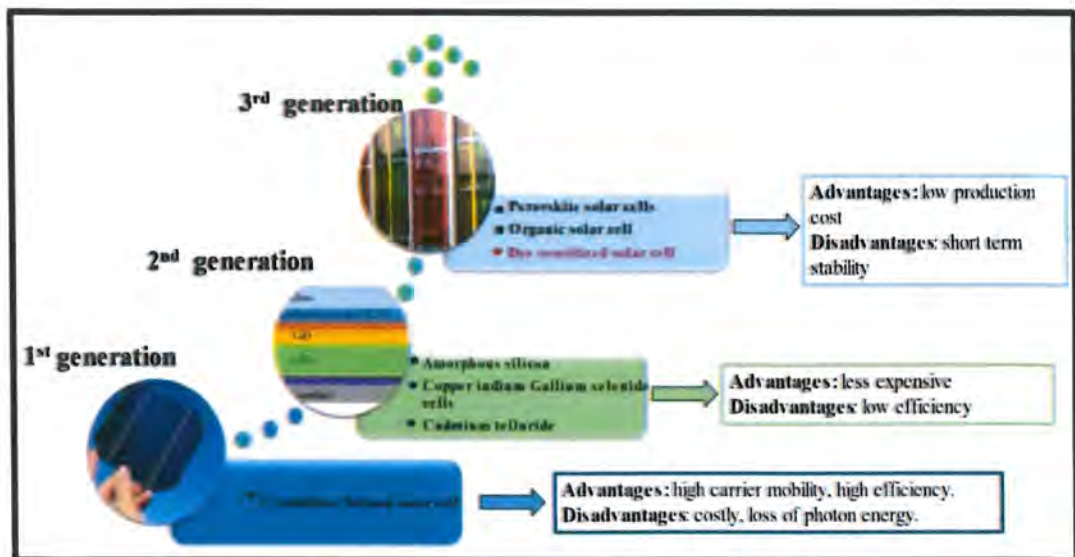
Figure. 1.6. Classification of photovoltaic devices.

1.6 Dye-Sensitized Solar Cells (DSSCs)

Michael Gratzel and O'Regan invented the first dye-sensitized solar cell by the combination of electrodes made up of semiconducting material (nanoparticles) and dyes for increasing charge transfer with efficiency of 7% in 1991[15].These cells are named as dye sensitized because they work in the presence of sunlight and uses a dye for capturing the light and enhancing the light absorption of the solar cells[16].

Their mechanism of generation and transportation of charge carries are the two important process that make them different form other solar cells. Working of dye sensitized solar cell is shown in the Figure 1.7.
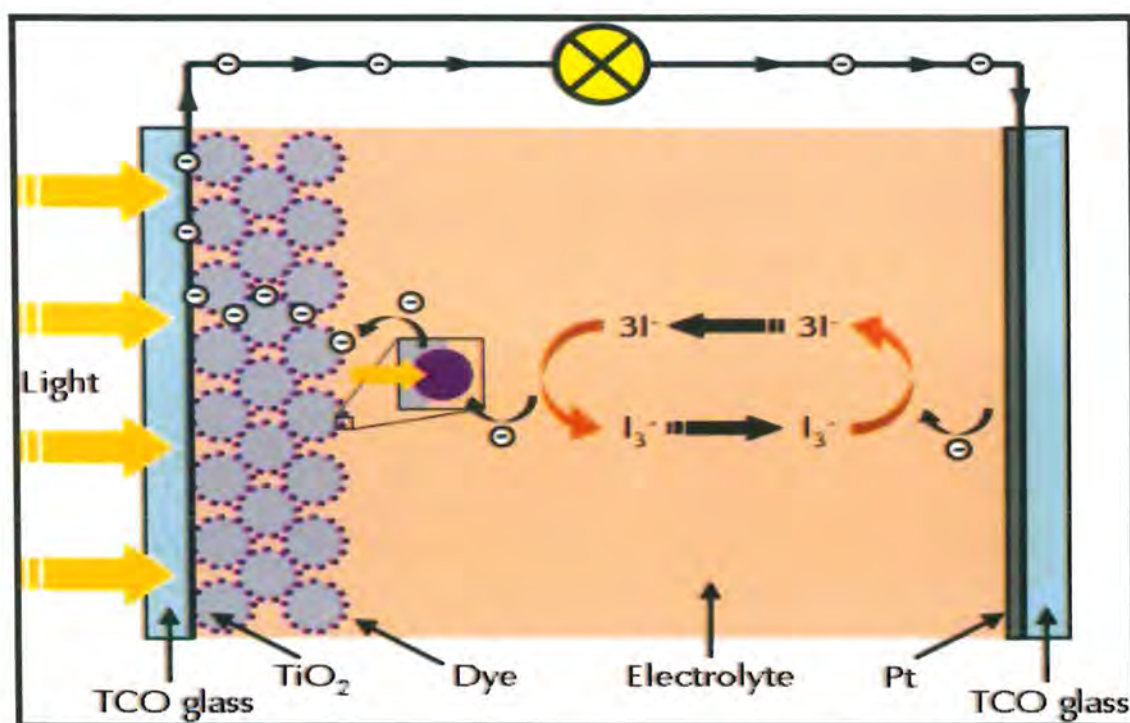
Figure. 1.7. Schematic representation of nanocrystalline Dye-Sensitized Solar Cells[17].

1.6.1 Working Principle of DSSCs

In DSSC, a transparent conducting oxide (ITO/FTO) act as working electrode on the surface of this mesoporous nanocrystalline TiO_2 is deposited, on this a sensitizer that is a dye is chemically adsorbed to capture photons of light. By the use of mesoporous nanocrystalline semiconducting material surface area of the semiconductor is increased so the greater number of dye molecules get absorbed to its surface to capture more light and photons so increasing the efficiency of solar cells[18].

8

Absorption of light is associated with the photoexcitation of the dye molecule and an electron is excited from HOMO to the LUMO of the dye molecule and then this electron the transferred from LUMO of the dye to the conduction band of semiconductor (conduction band of semiconductor should be at the lower energy than LUMO of the dye molecule) because of having porous semiconducting material the diffusion of electron to the conducting ITO substrate and hence to the electrode is made easy. Redox couple of the electrolyte helps to regenerate the dye by giving off the electron to the dye and itself gets oxidized the electron from working electrode after passing the external circuit comes to the counter electrode this electron is then accepted by the redox couple and the circuit is completed.

The important points for the efficient working of DSSCs

- Conducting glass substrate which is used for both the working and counter electrode, and which is responsible for the collection of electrons coming from photoanode and pass them to the counter electrode hence named as current collector, should be made of a transparent and low cost material having low electrical resistance. for example, FTO/ITO. A conducting glass substrate is used to enhance the light transmittance[19].

- Lager surface area nanocrystalline semiconducting material should be used to increase the amount of dye adsorbed because in case of single layer of dye molecules on the semiconductor less efficiency of solar cells has observed.

- Dye used should have high compatibility with semiconductor and should absorb in IR or visible region of solar spectrum and have good anchoring groups for strong chemisorption to the surface of semiconductor and effective electron transfer and most important thing is the dye stability in light and heat. And foremost it should be non-toxic and environment friendly.

- Electrolyte being the important component of DSSC, influences all the efficiency determining parameters of DSSC for example V_{oc} of the cell depends on redox potential of electrolyte, fill factor is affected by the diffusion rates of charge carriers in electrolyte. The stability of the cell is also dependent on the choice of electrolyte. So, selection of a compatible electrolyte is crucial.

- Counter electrode reduces the oxidized specie of redox couple and hence facilitates the dye regeneration it is generally a platinum deposited FTO electrode. This act as a catalyst for reduction of triiodide ion on cathode[20].

1.6.2 Fabrication of Dye-Sensitized Solar Cell

Following components are used for the fabrication of Dye-sensitized SolarCell as shown in Figure 1.8. these are:

1. Nanostructured Material (photoanode)
2. Organic sensitizers (dyes)
3. Electrolyte (containing the redox couple)
4. PEDOT: PSS (hole conducting polymer)
5. Counter Electrode (usually platinum/aluminum)
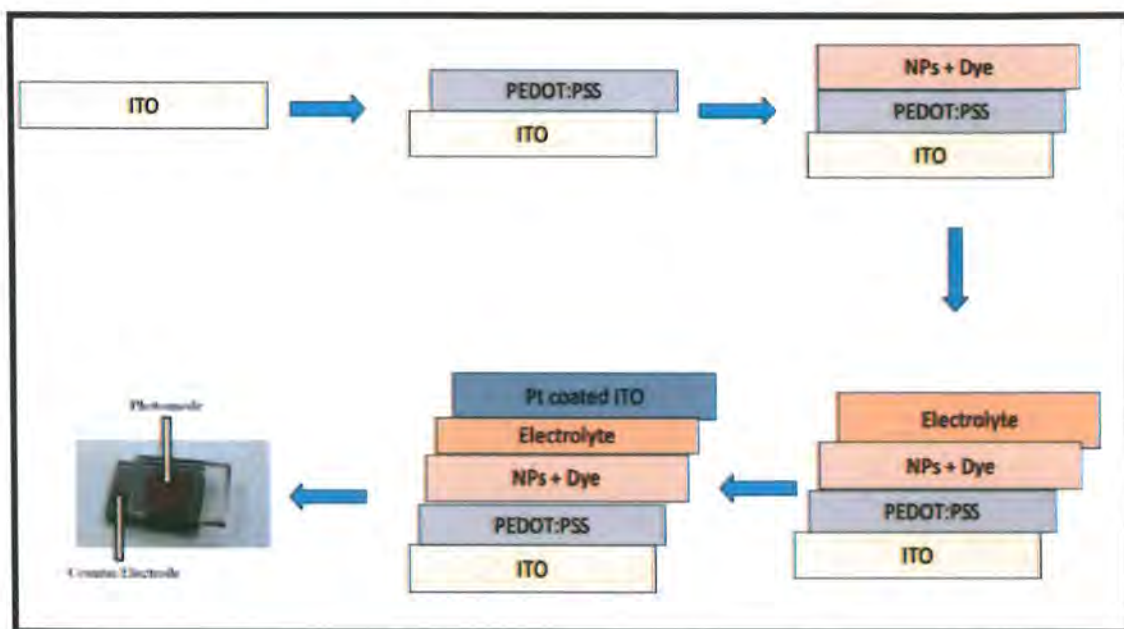
Figure. 1.8. Schematic representation of fabrication Dye-Sensitized Solar Cells.

1.7 Photoanode Material

Choice of semiconductor depends on the energy level compatibility between dyes and the semiconducting material. The choice is made based on:

- Band edge of conduction band.
- Effective electron transfers between dye and the semiconductor material.
- Particle size and morphology of the semiconducting material.

Conduction band of the semiconductor should lie below the LUMO of the dye for the effective electron transfer between them and for reducing the recombination chances of excited electron with the holes. Particle size and the morphology are the additional properties but are crucial because they dose effect the amount of dye

adsorbed on the surface of semiconducting material it has studied that in case of compact layer of semiconductor deposited on the conducting oxide surface, the surface area for the dye adsorption was less causing less number of photons toabsorbed and hence decreasing the cell efficiency while in the other case whenmesoporous material was used, it had more surface area allowing greater numbers of dye molecule to get adsorbed and increasing the total numbers of photons to get absorbed and hence increasing the efficiency of device, for this metal oxide paste is made using some binders for example polyethylene glycol and then coated on the substrate by different techniques available for strong adhesion on the glass plate.

For the removal of binder then these coated FTO/ITO glass plates are then annealed at high temperatures for almost 30 minutes leading to the formation of porous metal oxide coated moreover their morphology effects the transport of charge carriers to the working electrode or conducting metal oxide. The material to be used as photoanode semiconductor should have a wide band gap, higher electron mobility, longer lifetime of charge carriers, higher flat band gap and high stability against photo corrosion, should be non-toxic, easily available and less costly, till date different oxide semiconductors are used which are the commonly employedsemiconductors to set up porous anode. We can employ the other large band gap semiconducting material as photoanode in DSSCs for example the other transition metal oxide and check their efficiency in the cell and can also tune their properties such as structure, surface morphology, particle size and hence the related other properties like electrical conductivity, charge mobility and recombination chances by different process such as by doping with other metals, by making their composites with other metal oxides and so on[21].

1.8 Dyes as Photosensitizers

Dyes are the one of the most important components of dye sensitized solar cells and it helps to improve the efficiency of the cell which is the major target of the third generation solar cells[22]. Dye sensitization in DSSCs is required to:

- Improve the solar light absorption.
- Increase the number of charge carriers generated.

Different dyes have been employed for the sensitization of photoanode to broaden the light absorption spectra by the photoanode material they include:

- Metal Free Organic Dyes
- Natural Dyes
- Metal Organic Dyes

Dye used in the dye sensitized solar cell for the sensitization of photoanode should have some features these crucial features make them able to be used in DSSCs are:

❖ Better adsorption on the surface of photoanode for this it should have strongand large number of anchoring groups such as -COOH, -SO₃H etc.

❖ It should cover a range of sunlight spectra that is, can absorb photons in large range of wavelengths or energy to increase the efficiency of the cell.

❖ For easy electron transport LUMO of dye should be at higher energy level than that of conduction band of semiconductor.

❖ HOMO of dye should be at lower energy level than redox potential of electrolyte. Dye should not get aggregated on the photoanode surface otherwise it will have negative effect on solar cell efficiency.

❖ The last but foremost is the dye should be stable toward heat and light irradiation in the given set up. For this research work focus is on Carminic acid and Arsenazo III dye.

1.8.1 Carminic Acid Dye

Carminic acid is the red dyestuff which is commonly known as carmine or cochineal because it naturally resides in female cochineal. 15-20% carminic acid can be obtained from dried cochineal. Carminic acid is widely applicable in drinks, cosmetics, medicines, and foods. It is also being used in printing and dyeing of leather and wool.

Carminic acid is organic chromophore having the functionalities of phenolate and carboxylate and hydroxyl which provides sides for the attachment of semiconductor nanoparticles. Phenolate group behaves as electron donating group while carboxylate group act as main site for the anchoring of nanoparticles. Carminic acid is found as a good sensitizer because it readily attaches to the surface of nanoparticles by using its both carboxylate and hydroxyl anchoring groups. TheLUMO of carminic acid easily allow the directional flow of electrons into the conduction band of semiconducting nanoparticles[23].

The molecular formula of carminic acid is $C_{22}H_{20}O_{13}$ and structural formula is shown in Figure 1.9. The core of carminic acid consists of anthraquinone which is bonded to glucose unit structure. In 1990, carmine was first time prepared in laboratory by organic chemist.
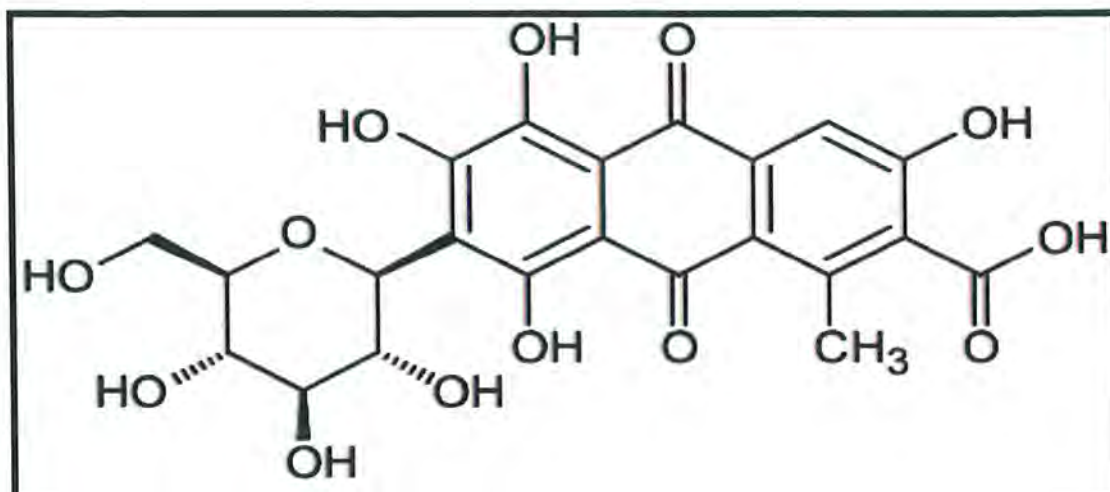
Figure. 1.9. Chemical structure of CA dye[24].

1.8.1.1 IUPAC Name of Carminic Acid Dye

According to the International Union of Pure and Applied Chemistry,Carmine Acid is named as:3,5,6,8-tetrahydroxy-1-methyl-9,10-dioxo-7-[(2S,3R,4R,5S,6R)-3,4,5-trihydroxy-6 (hydroxymethyl) oxan-2-yl]-9,10-dihydroanthracene-2-carboxylic acid.

1.8.1.2 General Properties of Carminic Acid Dye

Some common properties of carminic acid dye are given below:

❖ Molecular weight of carmine dye is 492.389 g/mol.

❖ Carminic acid dye is red to dark red in colour.

❖ It shows excellent stability in water, alcohol, ether, alkaline solution etc. but is insoluble in petroleum, benzene and chloroform.

❖ It decomposes at 136.11 °C.

❖ It is also used to impart red colour to different food additives and wool or leather.

❖ It is also playing role in pharmaceuticals biochemistry and solar cells.

1.8.2 Arsenazo III Dye

Arsenazo III dye is anionic azo dye. The majority of all colorants at least 66%

are found in the azo dye category, which make up the largest chemical class. The inclusion of one or more azo groups in their structure, together with hydroxyl groups, amine, and substituted amine groups acting as auxochromes, is what makes them distinctive. They have a wide range of applications[25].

S. B. Savin and V. I. Kuznetsov were the first to create the synthetic anionic azo dye known as arsenazo. Arsenazo III is found as a good photosensitizer because it readily attaches to the surface of nanoparticles owing to containing large number of anchoring groups responsible for chemisorption to the surface of nanoparticles.

Molecular formula of Arsenazo III is $C_{22}H_{18}As_2N_4O_{14}S_2$, and structural formula is shown in the Figure 1.10.
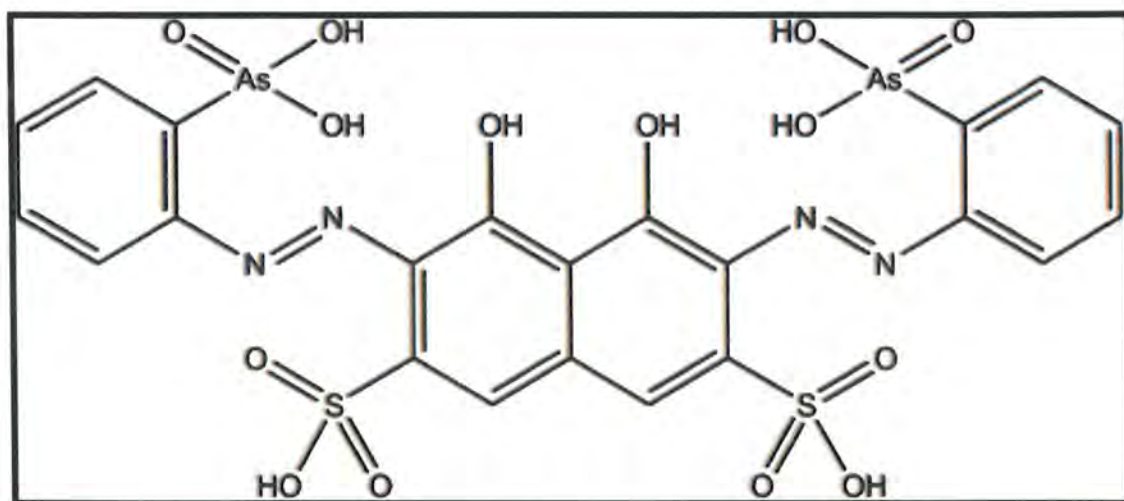
Figure. 1.10. Chemical structure of AZ dye[26].

1.8.2.1 IUPAC Name of Arsenazo III Dye

According to International Union of Pure and Applied Chemistry Arsenazo III dye is named as 2,2′-(1,8-dihydroxy-3,6-disulfonaphthylene-2,7-bisazo) bisbenzenearsonic acid.

1.8.2.2 General Properties of Arsenazo III Dye

Some general properties of Arsenazo III dye are:

❖ Molecular weight of Arsenazo III dye is 776.363 g/mol.

❖ Arsenazo III dye is present in powder form and normally at neutral pH it forms blue coloured complexes.

❖ It is soluble in water, ammonium hydroxide and alcohol.

14

❖ It is calcium sensitive dye, so a little amount of calcium is present as an impurity within it.

❖ It is frequently used in complexometric and photochemical determination of metal ions particularly lanthanides.

1.9 Electrolytes Containing Redox Couple

Electrolyte is a major component of DSSCs which is responsible for the regeneration of the dye and hence has major influence on the effectiveness of the cell. At the counter electrode redox couple should readily accept the electron while should barely accept the electron from working electrode. Electrolyte to be used in dye sensitized solar cells should possess some important characteristics which are:

❖ It ought to be reversible and chemically stable.

❖ For the quick diffusion of charge carriers, it should be viscous.

❖ It shouldn't cause the semiconductor material that is bonded to the FTO plate to disperse or the dye to desorb.

❖ It should readily accept the electron from counter electrode but not fromworking electrode.

The iodide/tri-iodide redox pair is the most prevalent, stable, and highly effective redox mediator. This redox mediator is promising since dye molecules regenerate quickly. With its low viscosity, insignificant vapour pressure, optimal boiling temperature, and dielectric characteristics, it is discovered to be the perfect electrolyte. Additionally, it possesses significant qualities including chemical inertness, environmental sustainability, and simplicity of processing. Iodide triiodideis the best electrolyte and shows the maximum efficiency because iodide ions are readily regenerated at the counter electrode while I^{3-} hardly accepts the electron from semiconductor, reduction of triiodide ion at the counter electrode take place as:

$$I_3^- + 2e^- \rightleftharpoons 3I^- \tag{1.1}$$

1.9.1   Oxidation and Reduction Reactions in Redox CoupleAt Anode

Dye + Light

(photons) $\longrightarrow$ Dye*(dye excitation) (1.2)

+ TiO$_2$ $\longrightarrow$ Dye$^+$ + electron injection to TiO$_2$ (1.3)

$$2 \text{ Dye}^+ + 3I \longrightarrow 2 \text{ Dye} + I_3^- \text{(dye regeneration)} \qquad (1.4)$$

At Cathode

$$I_3^- + 2e \longrightarrow 3I$$
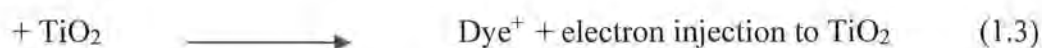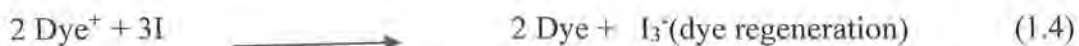
Iodide ions has serious issue regarding its volatility and Iodide/tri-iodide redox couple also has a negative side in that it can easily corrode substrates like silver and copper metal joints when employed as current collectors, and it can also decrease photovoltage due to its redox potential. When the dye is exposed to radiation, it also absorbs some photons and some visible light. So the investigation shifts to looking at some other iodide/tri-iodide mediator substitutes[27].

1.9.2 Disadvantages of Liquid Electrolytes

Liquid electrolytes can be used as electrolyte in DSSCs, but they have certaindisadvantages which make them unfit to be used in solar cell these are:

❖ Leakage and volatilization are the main problems that arise due to the use ofliquid electrolyte.

❖ They can cause dye desorption as well as photodegradation.

❖ They also control the lifetime of DSSCs by corroding the counter electrode.

To overcome this problem liquid electrolyte are being replaced by solid or quasi-solid electrolytes. The electrolytes are best for the development of Solid State Dye Sensitized Solar Cells (SSDSSCs) due to their excellent dealing capabilities[28].

1.9.3 Poly-3-hexylthiophene(P3HT) As Solid State Electrolyte

It is a p-type organic semiconducting polymer which is used in DSSCs. P3HT or poly-3-hexylthiophene belongs to polythiophene class. These are the polymers consisting of thiophene as a monomer. Thiophene is heterocyclic aromatic compound with sulfur as a heteroatom.

In solid state DSSCs, P3HT behaves as a good electrolyte as well as a hole conducting material. When it is doped with organic acids or halogens, it generates charge units which act as conductor or hole carrier[29].

P3HT shows maximum absorption at about 540-550 nm in organic solvents. Absorption spectrum of P3HT shows a bathochromic or hypochromic shift due to the length of conjugated system, when the length of conjugated system increases, the

absorption peaks shift towards the higher wavelength or show bathochromic shift which results in decrease in bandgap energy. Similarly, if the length of conjugated system lessens then peaks show hypochromic or blue shift which increases the band gap energy.

In solid state DSSCs, P3HT plays the same role as performed by liquid electrolyte[30].

P3HT plays two significant functions in DSSCs which are given below:

❖ Holes generated in dye molecules are accepted by P3HT and carried out toward counter electrode.

1.10 Counter Electrode

Counter electrode is a crucial component for the fabrication of dye sensitized solar cells there are different functions performed by the counter electrode which includes:

❖ The oxidized redox pair is reduced at the surface of the counter electrode by receiving electrons, which is one of the three crucial tasks of the counter electrode as a potential catalyst.

❖ It transports electrons from the outer circuit into the electrolyte solution of the inner cell. Thus, the counter electrode's primary function is to transmit electrons from the load to the cell for circulation.

❖ To maximize the use of sunlight, the counter electrode serves as a mirror and reflects any light that is not absorbed to the photoanode.

To perform these functions effectively counter electrode should possess some characteristics which are[31]:

❖ The counter electrode should have high catalytic activity.
❖ It should have high conductivity and reflectivity.
❖ It should have a high surface area with porous nature.
❖ chemical corrosion resistance.
❖ high chemical and mechanical stability.
❖ Its energy level should be compatible with potential of redox electrolyte.
❖ It should show good adhesiveness toward transparent conducting oxide substratein order to fulfill these fundamental functions.

In standard cells, platinum paste serves as the counter electrode material to complete the redox reaction. Carbon, graphite, and conductive polymers are employed as counter electrode materials in addition to platinum[32].

Platinum is still the best option for catalysts due to its simple iodide/tri-iodide redox kinetics. Counter electrodes are created using a variety of processes, including electro deposition, chemical vapor deposition, hydrothermal deposition, and sputtering.

1.11 PEDOT: PSS

The translucent poly (3,4-ethylenedioxythiphene) polystyrene sulfonate performs as a conducting polymer. It involves two ionomers in which first isomer is sulfonated polystyrene which possess negative charge after the removal of proton from sulfonate group and the second ionomer is the positive charge carrying PEDOT [poly(3,4-ethylenedioxythiophene)][33].

These two oppositely charged ionomers are responsible for producing a macromolecular salt. PEDOT: PSS shows the conductivity of approximately 1000 S/cm which can be improved by treating it with various compounds like acids, germinal diols, phenol and glycol. Thin layer of PEDOT: PSS is coated over the conducting ITO glass which enhances its stability as well as makes it smooth by stopping the diffusion of oxygen and indium through the anode.

PEDOT: PSS is used for:

❖ It is applicable as a transparent highly ductile and conductive polymer.
❖ It works as an electrolyte in polymer electrolytic capacitors.
❖ It is utilized as an antistatic agent in films and photography.

1.12 Nanotechnology and Nanoscience in DSSCs

Nanotechnology is advance and modern field of science and technology in which at least one dimension of particle should be in nanometer scale. Those materials having particle size ranging from 1-100 nm are called nanomaterials. This technology is getting importance in all the fields including physics, chemistry, and engineering. In the last decades, many advancements have been carried in this field by the synthesis of different nanotubes, nanobelts, nanoparticles and nanowires[34].

The efficiency of solar cell depends on the dye which is capturing the incoming photon. So, the dye is adsorbed on the photoanode, if photoanode is the nanomaterial

it will provide more surface area for the attachment of dye rather thanthe bulk photoanode. Hence, nanotechnology plays an important role in DSSCs.

These nanoparticles provide large surface area, so they are best to make photoanode being used in DSSCs. In nanocrystalline film-based electrodes, charge transfer is hundreds of times slower than electrodes made of nanowires[35]. Oxide aggregates are also used as nanomaterials in dye sensitized solar cells[36]. These aggregates are prepared by clustering of nanoparticles and ranges in size of microns[37].

Nanomaterials are of four types depending on their structure and sizes. These types are given below:

1   Nanoparticles provide large surface area for the adsorption of dye with photoanode but also increases chances of renominations of charge carriers.

2   Nanowires and nanotubes are responsible to provide straight direction for charge carriers transportation but have smaller surface area for the dye adsorption at the anode.

3   Core-shell structures, although they are less stable and least effective, but they reduce the chances of charge carrier recombination.

4   Aggregates of oxides provide large surface area as well as also scatters the visible light of solar spectrum.

1.12.1 Synthesis of Nanostructured Material

There are two ways for the synthesis of Nanostructured materials[38]. By using these methods, nanostructures of definite shape, crystalline size and structures can be made. These methods are given below:

1.12.1.1 Top-Down Method of Synthesis of Nanomaterial

In this method, size of bulk material is reduced up to range of size of the nanomaterial to change bulk into nanoparticles. Some top-down approaches for nanomaterial synthesis include:

- Spray of Aerosol[39]
- Electron Beam Lithography[40]
- Mechanical Milling[41]
- Atomic Force Microscopy[42]
- Condensation of Gas Phase[43]

- Etching
- Sputtering[44]

Nanostructured materials synthesized by these methods may have some crystallographic defects and non-smooth surface due to Prescence of impurities which reduces the electrical conductivities.

1.12.1.2 Bottom-Up Method of the Synthesis of Nanomaterial

In this method, nanomaterials are synthesized by joining one atom with other to form molecules or clusters. Compared to top-down approach this is more attractive method for nanoparticles synthesis because size and the other properties of nanomaterials are more controllable in this case of synthesis.

Some bottom-up methods for the synthesis of nanomaterials include:

- Sol-gel Method[45]
- Vapor-Phase Deposition Approach[46]
- Hydrothermal Synthesis Method[47]
- Wet chemical Synthesis[48]
- Laser Pyrolysis
- Chemical reduction[49]

There are less chances of crystal and structure defects of nanomaterial in thisapproach of synthesis.
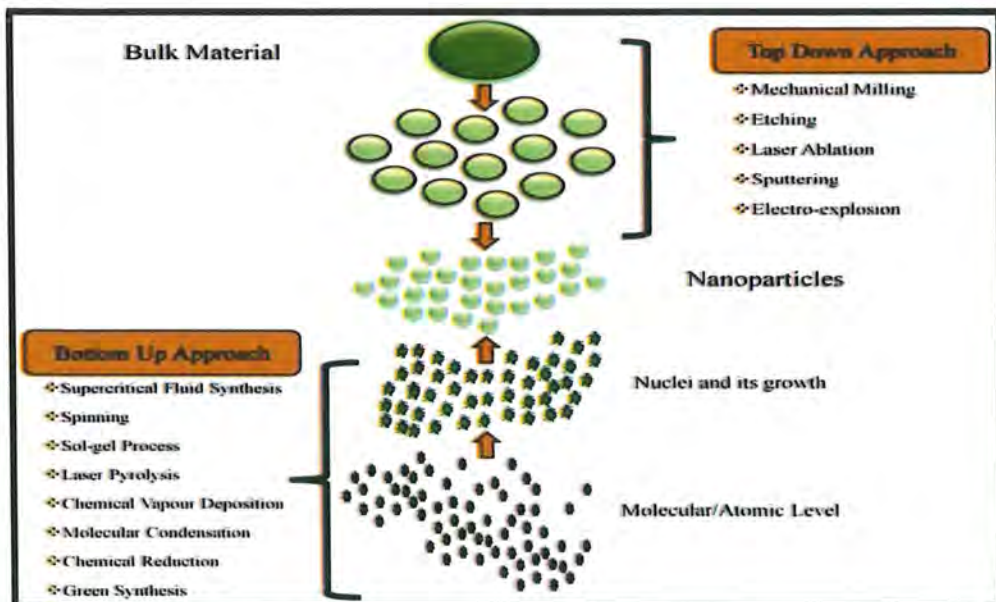

Figure. 1.11. Method for the synthesis of nanostructure material[50].

1.13 Characterization Techniques

20

Characterization of the nanomaterials was done by using different instruments. The working principles of these device are given below:

1.13.1 UV-Visible Spectroscopy

UV-Visible spectroscopy is a characterization technique used to determine the optical properties of the nanostructured materials. The double beam spectrophotometer is used for this purpose. It consists of light source, sample holder, detector, and a monochromatic.

UV-Visible is carried in the range of 200-800 nm in which UV region ranges from 200-400 mm while the visible region extends from 400-750 nm. Sample holders are made of quartz having 1cm thickness and reference is set according to the solvent selected for the preparation of the sample to run in double beam spectrophotometer. Shimadzu UV- 1800 spectrophotometer was used in this research work.
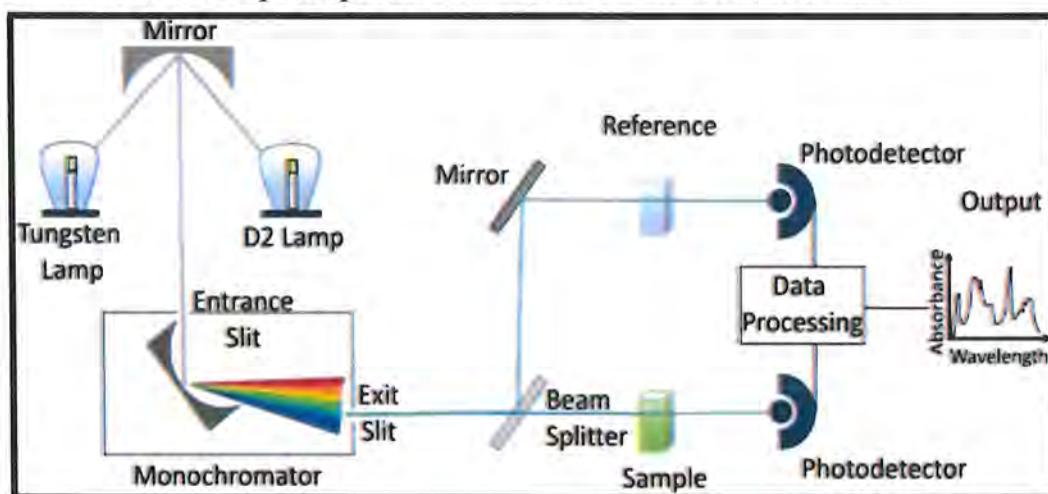
Figure. 1.12. Schematic representation of UV-Visible spectrophotometer[51].

1.13.2 X-Ray Diffraction Crystallography (XRD)

XRD works on the principle of Bragg's law ($n=2d\sin\theta$). It involves three components, X-Rays, tube detector and sample holder, for its operation. Electrons from the heated filament are subjected on the sample. These accelerated electrons knock out the inner electrons from the sample and hole is generated. This hole is occupied by the electrons jumping from the higher energy level into lower energy level followed by the emission of the rays known as X-rays. When these x-rays pass through the sample detector detects these radiations and are processed by the computer.
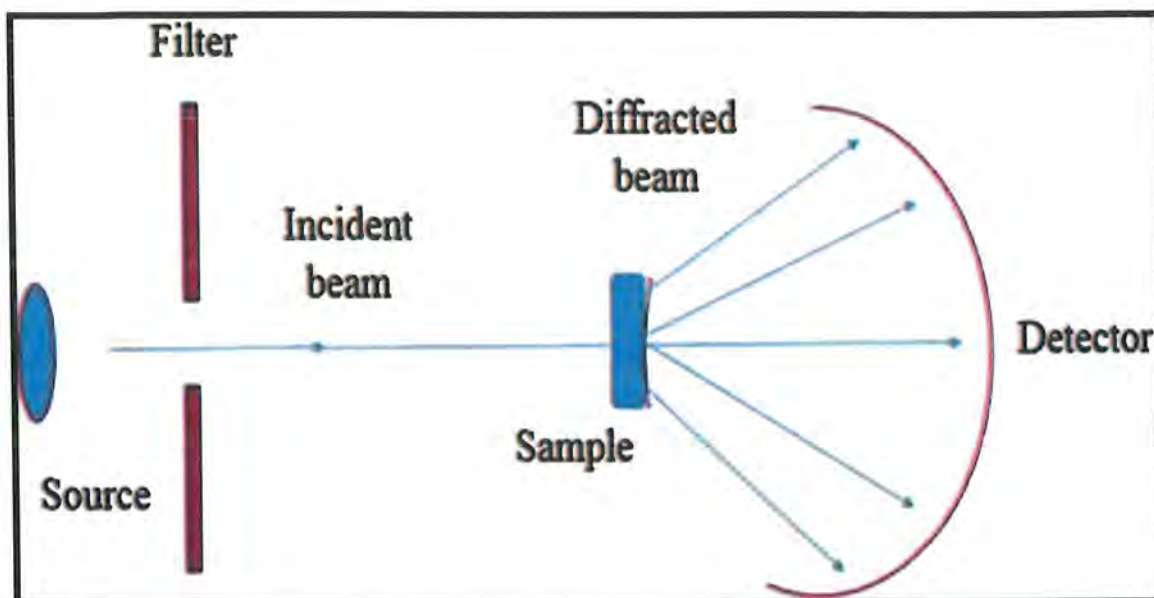
Figure. 1.13. Schematic representation of XRD analysis[52].

XRD is used to determine:

- Average crystallite size
- Crystallographic orientation
- Impurities in material
- Phase of crystallite size

Powdered sample is used for XRD analysis, and 0.05/min scan rate is applied to record the pattern in the range of angle from 20°-80°. X'Pert PRO PANalytical X-ray Diffractometer was used to calculate average crystallite size. Debye Scherrer Equation is used to determine the average crystallite size. This equation is:

$$D= K\lambda/\beta\cos\theta \qquad (1.5)$$

1.13.3 Fourier Transform Infrared Radiations (FT-IR) Spectroscopic Analysis

FT-IR is used to identify the compounds, impurities in sample as well as it alsomeasures the vibrational frequencies of the bonds in the given molecules. It works in the IR region so different functional groups show peaks in different regions corresponding to their bending and stretching modes. FT-IR spectrum is a graph between the transmittance and wavenumber along y-axis and x-axis respectively.Nanoparticles and

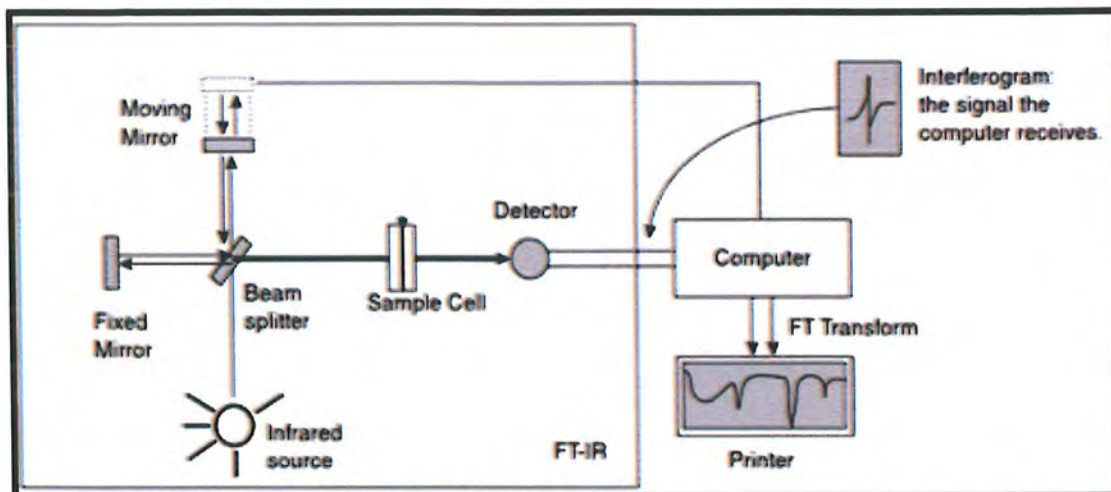their nanostructured materials show peak in the range of 400-1000 cm^{-1}.

Figure. 1.14. Schematic Representation of FT-IR Spectrophotometer[53]

Pure semiconducting materials and their nanostructured materials were characterized by FT-IR. Their spectrums showed peaks in given range which ensured their synthesis. The FTIR of dye before and after the grafting was also performed by F-510 FT-IR Spectrometer.

1.14 Literature Review

As energy is the key component for life so by increasing population and technology demand of energy is also increasing which results in the depletion of non-renewable resources i.e, fossil fuel, coal, natural gas etc. According to an estimate the reservoirs of oil throughout the world would last for 40 years while for natural gas and coal would remain for 60 years and 200 years respectively. This energy crisis urges researchers to replace the non-renewable resources by cheap and abundant renewable resources to fulfill basic energy demands. The Sun is the abundant, non-stop, reliable, and continuous supplier of energy thus the perception forenergy conversion was introduced by photovoltaic effect. Initially silicon based solar cells or conventional solar cells were used but due to high cost nowadays dye sensitized solar cells are more efficient because they are easy to fabricate at ambient temperature, on flexible substrates, show compatibility with roll-to-roll processing" and are made of inexpensive nanomaterials, nanorods or thin films with 11-13% efficiency". Different metal oxides (TiO_2, PbO_2, ZnO, Ga_2O_3, SnO_2, In_2O_3, CdO) were used in DSSCs due to their unique optical, morphological or electrical properties"[54]. Cerium oxide (CeO_2) is a n-type semiconductor having excellent optical and electrical properties, highly chemically stable, having tunable high band gap energy of E-3.2 eV, rapid production of charge carriers in the presence of sunlight, have high extinction coefficients and various stable morphological forms[55]. As band gap of cerium oxide is high it results in very few oxidative holes in UV region of light, inthe valence band (V.B) of cerium oxide which is responsible for the long- term stability of CeO_2 based dye sensitized solar cells. Moreover, CeO_2 show higher electron mobility rather than TiO_2 (0.1-1 cm V's. Due to its unique properties, it is applicable in optoelectronic devices[56] as photoanode in DSSC, as gas sensor or as anodic material in lithium-ion batteries. Cerium oxide nanoparticles have been synthesized by various methods which involves thermal evaporation, laser ablation method, calcination process, co-precipitation methods, chemical vapor deposition (CVD)[57], hydrothermal"[58], and carbothermal reduction methods. CeO_2 nanoparticles are being widely used in DSSCs as photo anodes but

24

show low photo conversion efficiency than common choices like TiO_2 because of its some intrinsic limitations as lower conduction band (C.B) energy as well as isoelectric point.

As the conduction band energy is low so chances of charge recombination increase, which also lowers the open circuit voltage (V_{oc}), major parameter of concern. The conduction band edge of CeO_2 is 0.3- 0.5 V lower than the TiO_2 which results in lower open circuit voltage V_{oc} and efficiency. Thus, to revive CeO_2 to get better results different strategies have been used i.e., core-shell nanostructured materials,[59] Nano composites formation or doping[57] etc. to increase the fermi energy level, enhance the chances to uptake the dyeand lessen the charge recombination. By these improvements in CeO_2, CeO_2 based dye sensitized solar cells employed high efficiency as TiO_2 based solar cells. Efficiency of CeO_2 has been enhanced by doping as well as composite formation in different ratios. In this research work, doping of nanoparticles is carried out to overcome the drawbacks of CeO_2. Zr has been selected for doping purpose because it has seen that by doping with transition metal like zirconium modifies the electricaland optical properties of the cerium oxide and enhances its efficiency to be used as photoanode in dye sensitized solar cell.

Chapter 2 MATERIALS AND METHODS

2.1 Chemicals

For the synthesis of pure and doped CeO_2 nanoparticles the following chemicals were used that are listed in Table 2.1 along with their chemical formulas, molar masses, percentage purities, densities and supplier names.

Table 2.1: List of chemicals and dyes used for the synthesis of pure and doped CeO_2 NPs.

Sr. No.	Name of compound	Chemical formula	Molar mass (g/mol)	Density (g/cm³)	Percentage Purity	Supplier
1	Cerium-nitrate hexahydrate	$Ce(NO_3)_3. 6H_2O$	434.22	1.67	99%	Sigma Aldrich
2	Sodium hydroxide	NaOH	40.0	2.13	99%	Sigma Aldrich
3	SalicylicAcid	HOC_6H_4COOH	138.12	1.44	99%	Sigma Aldrich
4	Zirconyl Chloride	$ZrOCl_2$	178.13	1.91	99%	Sigma Aldrich
5	ArsenazoIII	$C_{22}H_{18}As_2N_4O_{14}S_2$	776.36	0.85	98%	Sigma Aldrich
6	CarminicAcid	$C_{22}H_{20}O_{13}$	492.38	1.90	99%	Sigma Aldrich

2.2 Synthesis
2.2.1 Synthesis of Pristine Cerium Oxide NPs

For the synthesis of pure cerium oxide nanoparticles, co-precipitation method was used. In a two neck round bottom flask, 1.0 g of $Ce(NO_3)_3. 6H_2O$ was dissolved in 25mL of deionized water. NaOH solution was prepared by dissolving 1.2 g of NaOH in 100 mL of deionized water under constant stirring till sodium hydroxide was dissolved. 1 g of salicylic acid solution was formed in 20 of deionized water and then

it was added into the main solution. Dropwise added NaOH solution into the $Ce(NO_3)_3$. $6H_2O$ + salicylic acid solution with continuous stirring till Ph reaches 12 and yellowish-brown color precipitates begin to form gradually, and the solution becomes yellowish brown in color. This solution was stirred at 70 °C for 24 hours under constant magnetic stirring at moderate speed. Obtained precipitates were filtered and then washed with deionized water and methanol several times. Dried the sample in oven at 70 °C for 12 hours. The sample was grinded and calcined at 500°C for 3 hours. Yellowish white colored CeO_2 nanoparticles were obtained.
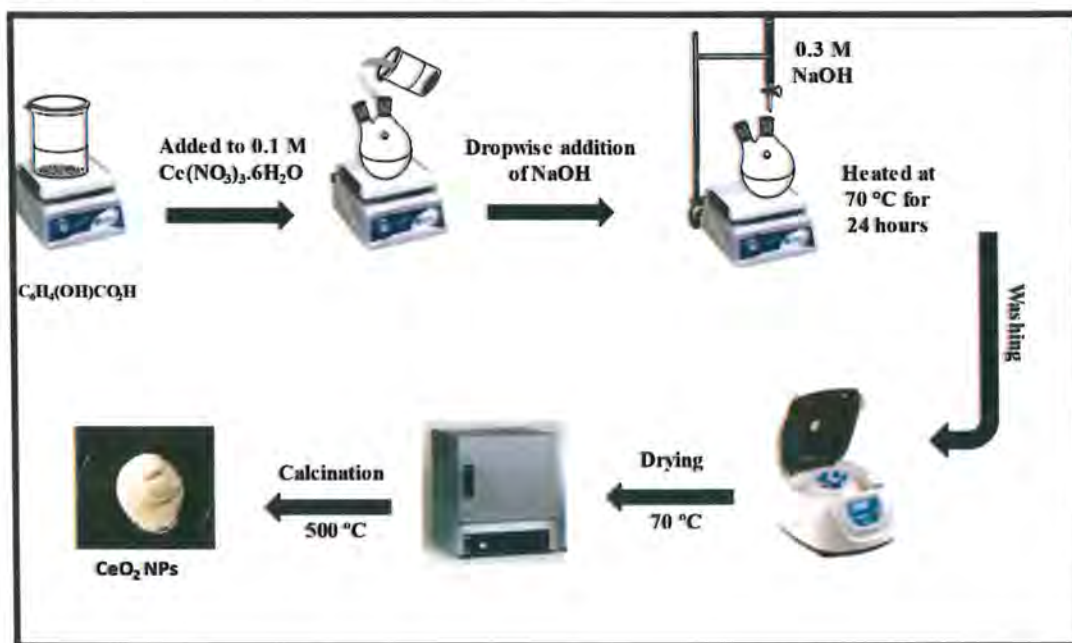
Figure. 2.1. Flow sheet diagram for synthesis of CeO_2 NPs.
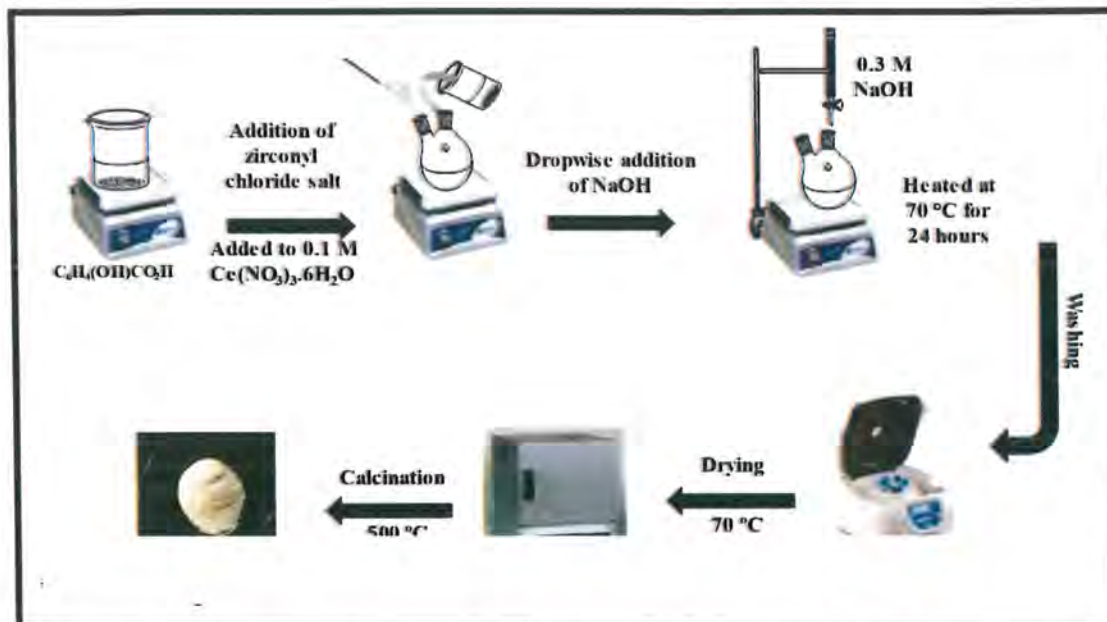
2.2.2 Synthesis of Zirconium Doped Cerium Oxide NPs

For the synthesis of zirconium doped cerium oxide nanoparticles, first of all added weight (1-6)% of zirconyl chloride in deionized water and stirrer to get a homogenous solution. After that solution g of cerium nitrate hexahydrate was added in it. 0.3 M sodium hydroxide solution was added into it dropwise till pH reaches 12. Repeated the same process that is written above. It resulted in the formation of (1-6)% composition of zirconium doped cerium oxide nanoparticles of different percentages.

Figure. 2.2. Flow Sheet Diagram for Synthesis of Zr Doped CeO$_2$ NPs.

Sensitization of Nanoparticles with dye solution

The surface of cerium oxide and zirconium doped cerium oxide nanoparticles were photosensitized using carminic acid dye and arsenazo III dye solutions separately. Carminic acid and arsenazo III dyes were found to be soluble in deionized water. Solutions of different concentrations of both the dyes were made separately for the purpose of photosensitization of nanoparticles.

2.2.3 Grafting of Carminic Acid Dye on Nanoparticles

Grafting is a chemisorption phenomenon which was carried out by the sensitization of nanoparticles with carminic acid. It involved following steps:

• In the first step, solution of 1mg of nanostructured material in 3ml of deionized water as a solvent was prepared. The solution was sonicated for 30 minutes to make a homogeneous solution.

• Different concentrations of carminic acid dye are prepared in deionized water. 3 mL of any of the prepared solution was added into the prepared solution of nanostructured material.

• After adding the dye solution, the solution was placed on hot plate for stirring under dark conditions to allow the carminic acid dye molecules to completely deposit on the surface of the nanostructured materials.

• Similarly, grafting was performed for all the dilutions of dye one by one in dark.

28

2.2.4 Grafting of Arsenazo III Dye on Nanoparticles

Sensitization of nanoparticles with the arsenazo III dye involved the following steps:

- In the first step, a solution of 1mg of nanoparticles in 3ml of deionized water is prepared, the solution was then sonicated to make it homogeneous.

- Different concentrations of arsenazo III dye were prepared in deionized water. 3ml of any of the prepared solution was added into prepared solution of nanoparticles.

- After adding the dye solution, the solution was placed on the hot plate for stirring under dark conditions to allow the arsenazo III dye to completely get grafted on the surface of nanoparticles.

Similarly, grafting was performed for other dilutions of dye one by one in dark.
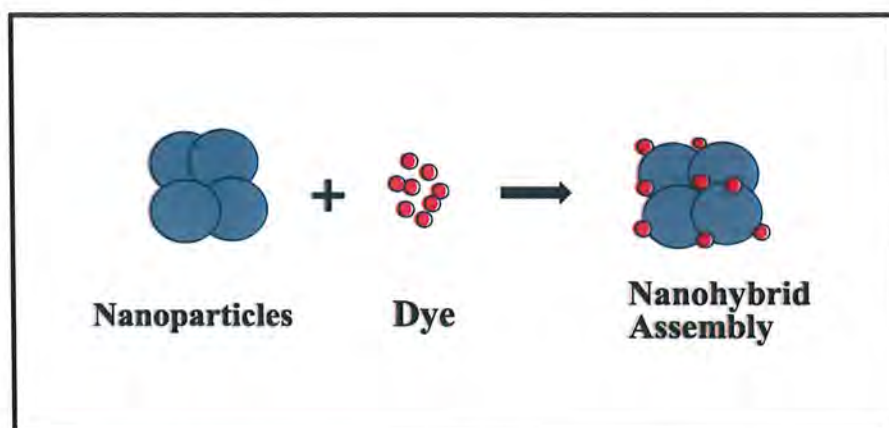
Figure. 2.3. Nanohybrid assembly of nanostructured material and dye.

29

Chapter 3 Results and Discussions

As discussed in the experimental section, nanoparticles were synthesized by co-precipitation method. In this chapter several techniques were employed for their optical and morphological characterizations.

3.1 Optical and Morphological Characterization of Nanostructured Materials

Optical and morphological properties of nanoparticles and their nanostructured materials were analyzed through various characterization techniques which include:

- UV-Visible Spectroscopy
- X-Ray Diffraction Analysis
- Fourier Transform Infrared (FT-IR) Spectroscopy

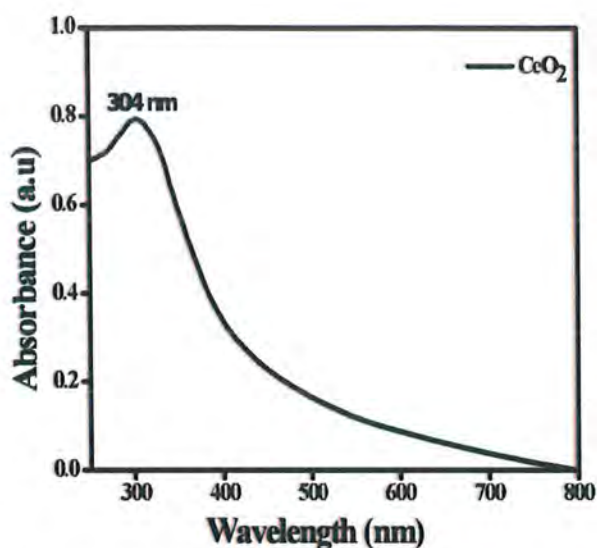### 3.1.1 UV-Visible Spectroscopy

UV-Visible spectrophotometer was used to perform UV-Visible spectroscopy of nanomaterials. It was used to determine the optical properties of nanoparticles. The UV-Visible spectroscopic analysis was done in the wavelength range of 2 00 to 750nm. The samples were prepared by using deionized water as a solvent. Absorption spectrum data helped in the estimation of band gaps of samples by using tauc plots. The material's optical band gap energy can be obtained by extrapolating the linear portion of the absorption curve.

3.1.1.1 Optical Properties of Pure and Zr- CeO$_2$ Nanoparticles

The UV-Visible absorption spectrum of CeO$_2$ nanoparticles is shown in Figure

3.1. The spectrum showed the absorption peak at 304 nm.

Figure.3.1. UV-Visible spectrum of CeO2 NPs.

The band gap energy of pure CeO_2 calculated by Tauc's plot method comes outto be 3.25 eV and it is shown in Figure 3.2.
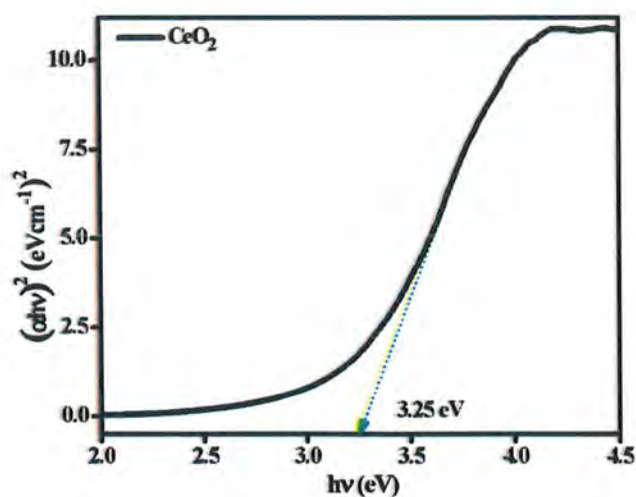
Figure. 3.2. Tauc plot of CeO2 NPs.

The absorption spectra of pure and (1-6)% Zr-doped CeO_2 nanoparticles is shown in Fig. 3.3. Pure and Zr-doped CeO_2 nanoparticles possess strong absorption peaks in the range of (292-339) nm. 1% zirconium doped CeO_2 NPs shows the maximum absorption peak at 314 nm and the band gap is at 3.08 eV.
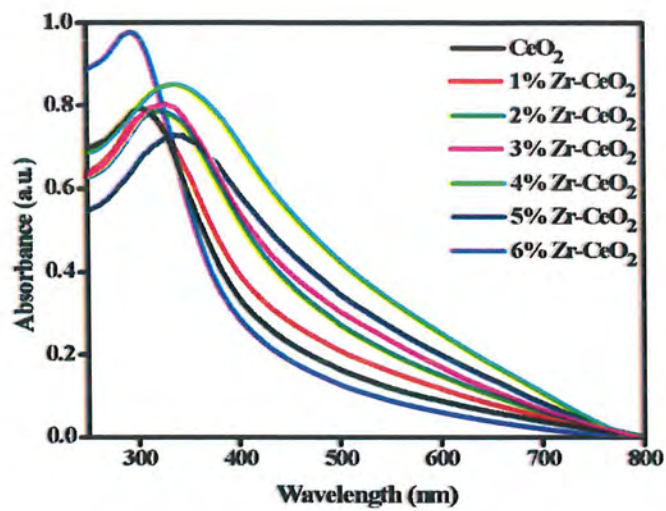
Figure. 3.3. UV-Visible spectra of pure and Zr(1-6)% doped CeO$_2$ nanoparticles.
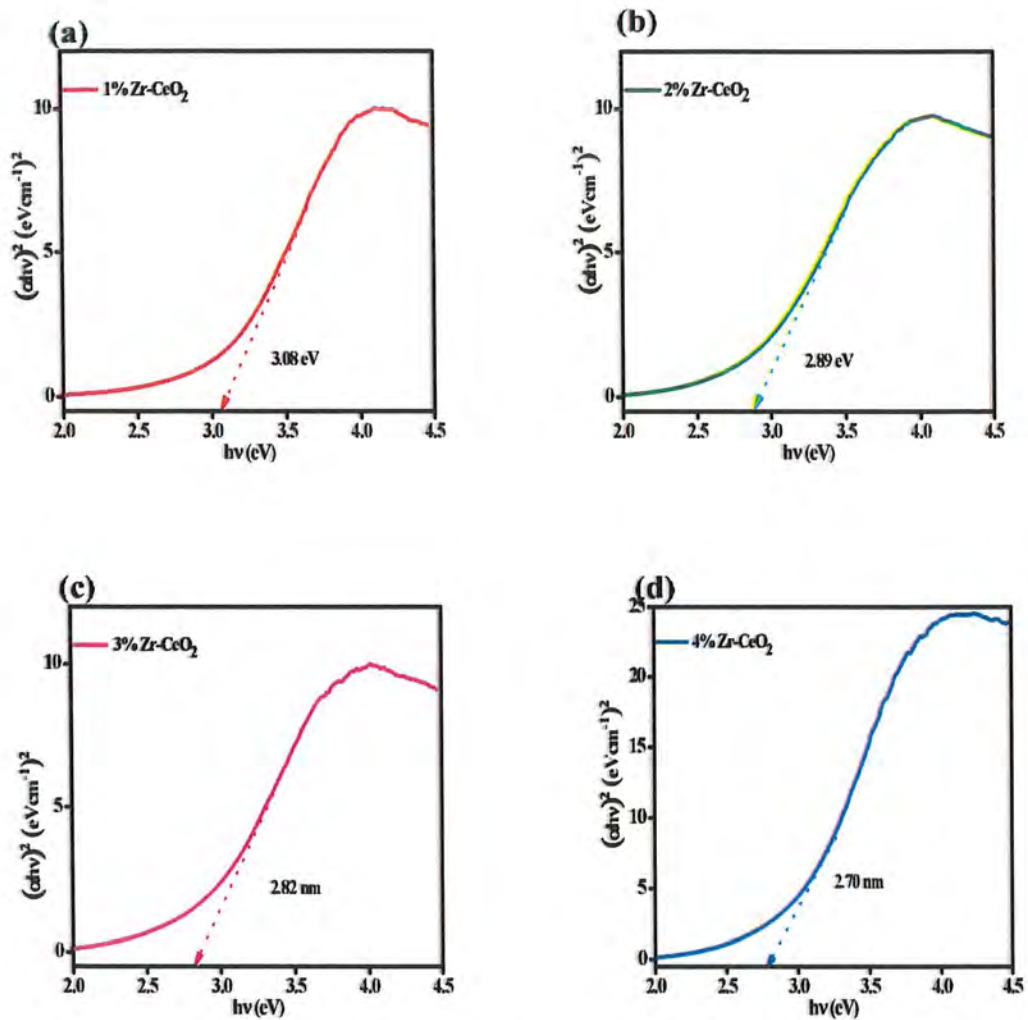
Figure. 3.4. Tauc plots of (a) 1% Zr-CeO$_2$ (b) 2% Zr-CeO$_2$ (c) 3% Zr-CeO$_2$ (d) 4%Zr-CeO$_2$.
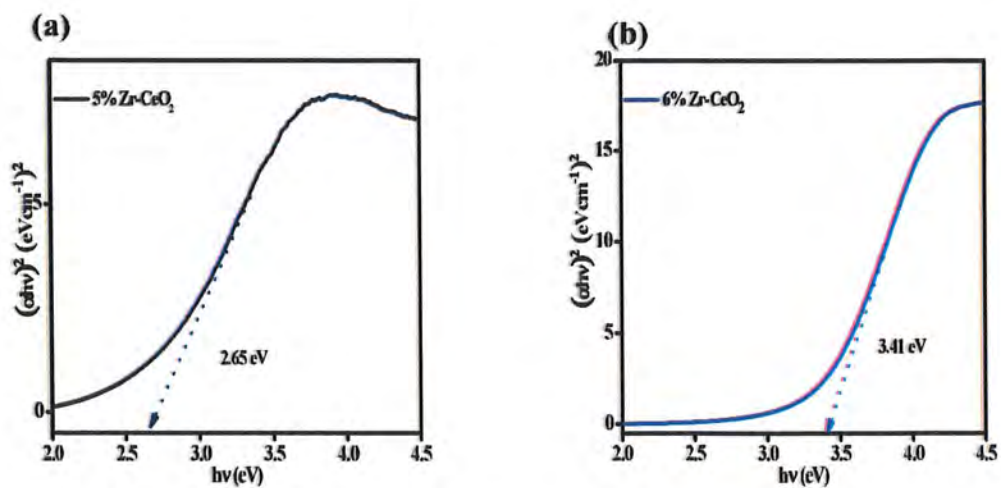
Figure. 3.5. Tauc plots (a) 5% Zr-CeO$_2$ (b) 6% Zr-CeO$_2$.

Figure 3.4. shows the tauc plots of pure and doped nanoparticles which confirmed a slight red shift in the absorption peaks that cause narrowing of energy band gap. The maximum absorption peaks for the 2% and 3% Zr-CeO$_2$ were at 319 nm, 322 nm respectively and band gap values for these samples were at 2.89 eV to 2.82 eV respectively, tauc plots for 2% and 3% Zr-CeO$_2$ are shown in Figure 3.4 (b) and 3.4 (c) respectively. This shows an increase in wavelength which resulted in the decrease in the band gap energy known as red shift. Similarly, the maximum absorption peaks for 4% and 5% Zr-CeO$_2$ were at 330 nm and 339 nm respectively while the band gaps of the samples calculated from the tauc plots are 2.70 eV and 2.65 eV. the tauc plots of 4% and 5% Zr-CeO$_2$ are shown in Figure 3.3 (d) and 3.4 (a). This occurs due to new energy levels created by Zr due to charge transfer between dopant and material, so the band gap falls. Illustrated according to this relation.

$$E = hc/\lambda \qquad\qquad (3.1)$$

The absorption spectra for the 6% Zr-CeO$_2$ NPs shows maximum absorption peak at 298 nm. It shows a reduction in wavelength which indicates blue shift or bathochromic shift and as a result there is an increase in band gap energy that is 3.41 eV. This occurs due to quantum size confinement that decreases the particle size and as a result deformation of the CeO$_2$ lattice structure takes place. This is also explained by the Burstein Moss effect according to which after a certain concentration of dopant, all the fermi levels in conduction band were occupied so excited electron move to the conduction band above the fermi levels and as a result there is an increase in band gap. The values of maximum absorption peaks and their respective band gaps of the zirconium doped CeO2 NPs are given in Table 3.1.

Table 3.1: Maximum absorption peaks and respective band gaps of the zirconium doped
CeO_2

Sr. No.	Sample	Maximum Absorption Peak (nm)	Band gap (eV)
1	CeO_2	304	3.25
2	1% Zr- CeO_2	314	3.08
3	2% Zr- CeO_2	319	2.89
4	3% Zr- CeO_2	322	2.82
5	4% Zr- CeO_2	330	2.70
6	5% Zr- CeO_2	339	2.65
7	6% Zr- CeO_2	292	3.41

3.1.2 X-Ray Diffraction (XRD)

The XRD pattern of pure CeO_2 nanoparticles is shown in the Figure 3.3. The crystallographic planes (111), (200), (220), (311), (222) and (400) corresponds to the detected diffraction peaks at 2θ values of 28.61°, 33.14°, 47.55°, 56.47°, 59.04°, and 69.45°, respectively. The diffraction peaks confirm the formation of CeO_2 singlephase. The sharp and broad peaks of the CeO_2 were may be a result of the crystalline structure of pristine CeO_2 shown in Fig 3.5. The peaks satisfactorily met the Joint Committee on Powder Diffraction Standards (JCPDS) requirements (Reference file no. 34-0394)
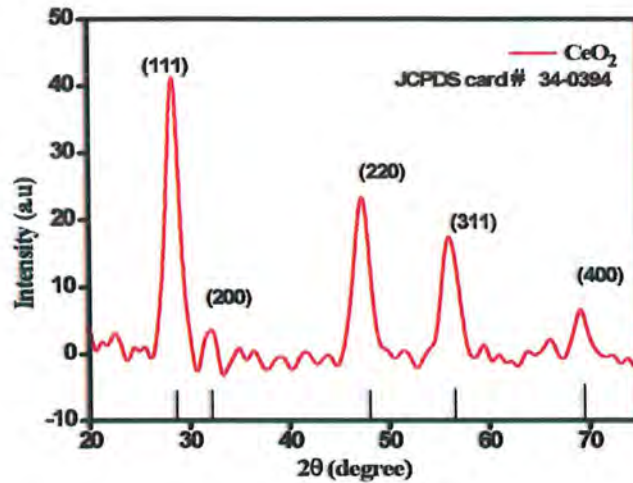
Figure. 3.6. XRD pattern of pure CeO₂ NPs.

The Debye Scherrer equation is used to calculate the average crystallite size ofthe nanomaterials. This equation is:

$$D = K\lambda / \beta Cos\theta \quad (3.2)$$

Here,

D= Average crystallite size

K= Dimension shape factor=0.9

λ = X-ray wavelength = 0.154 nm

β= FWMH (Full Width at Half Maximum)θ= Bragg s angle

The average crystallite size of CeO₂ nanoparticles calculated by this equation comes out to be 11 nm. XRD patterns of pristine CeO₂ and Zr doped CeO₂ NPs as shown in Figure 3.5. No impurity peaks or zirconium related phases were found after zirconium doping of CeO₂ NPs.
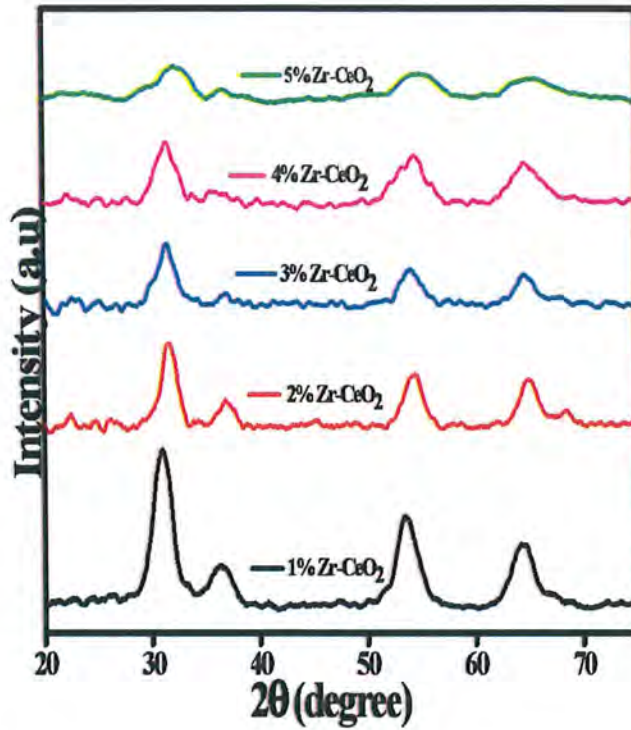
Figure. 3.7. XRD patterns of Zr(1-5)% doped CeO₂.

Additionally, it was observed that when the concentration of zirconium rises, the most intense peak gradually widened and shifted to a higher angle. According to Bragg's equation,

$$n\lambda = 2d\sin\theta \qquad (3.3)$$

This equation shows the inverse relation between d-spacing (d) and diffractionangle (θ). Widening of peaks and shifting towards higher 2θ values is because of decrease in d-spacing between planes. This occurs due to difference in ionic radius of Zr and Ce ions. As the ionic radius of Zr is less than Ce, so it causes a decrease in d- spacing which will shift the peak values to a higher angel.

Table 3.2: Average crystallite size of pure CeO_2 and Zr doped CeO_2.

3.1.3 Fourier transform infrared spectroscopy (FT-IR)

FT-IR spectroscopy was carried out in the range of 400 cm^{-1} to 4000 cm^{-1}. It

S.No.	Samples	Crystallite size(nm)
1	CeO_2	11.5
2	1% Zr- CeO_2	10.0
3	2% Zr- CeO_2	9.2
4	3% Zr- CeO_2	8.5
5	4% Zr- CeO_2	7.6
6	5% Zr- CeO_2	7.1

ensured the synthesis of nanostructured material by showing characteristics peaks of the material. FT-IR spectrum of pure CeO_2 nanoparticles is shown below. In FT-IR spectrum a strong peak appears at 3200 to 3500 cm^{-1} which is due to stretching of hydroxyl group of water absorbed on the surface of synthesized nanoparticles. The peak at 2359 cm^{-1} is due to the vibrations of atmospheric CO_2. The peak at 1530 cm^{-1} corresponds to bending vibrations of O-H bond, metal oxide bonds in FT-IR spectra appear in the range of 400-900 cm^{-1} and while the characteristic peak of Ce-Oappeared at 468 cm^{-1}.
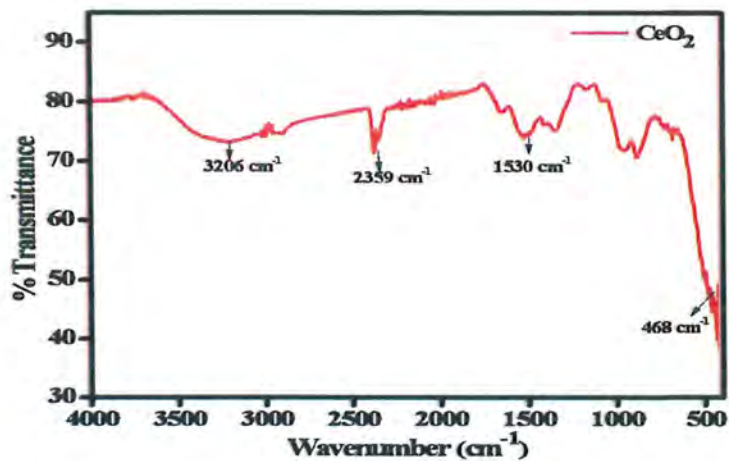
Figure. 3.8. FT-IR spectrum of pure CeO$_2$.

FT-IR spectra of doped materials is also shown below, in this spectrum the zirconium doped ceria nanoparticles did not show any extra peaks because as wavenumber at which bond vibrates is inversely related to the reduced mass of the bonded atoms, so if the vibration of bond involving zirconium atom might be towards the lower wavenumber number and not clearly observable in the spectra. while if we compare the spectrum of doped material with that of pure ceria nanoparticles, all other peaks are the same.
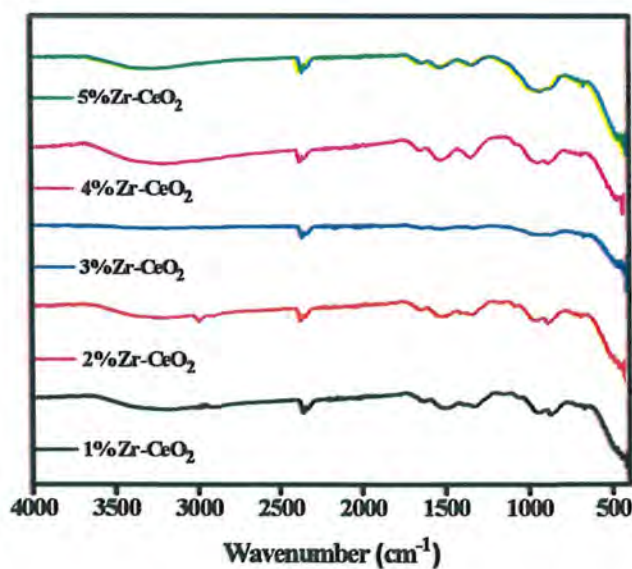

Figure. 3.9. FT-IR spectra of zirconium doped ceria nanoparticles.

3.2 UV-Visible Spectroscopy of Pure Dyes

3.2.1 UV-Visible Spectrum of Carminic Acid

In this research work carminic acid and arsenazo III dye was used as a photosensitizer which is essential component in DSSCs. UV-Visible spectroscopy of dye solution prepared in water as a solvent was performed.

In UV-Visible spectrum of the dye carminic acid a broad peak was observed in the range of 450-580 nm while a sharp peak was observed at 272 nm. The broad peak in the spectrum was due to the n-π* transitions while the sharp peak appeared due to the π- π* transitions. The UV-Visible spectrum of the carminic acid dye is shown in the Figure 3.8.
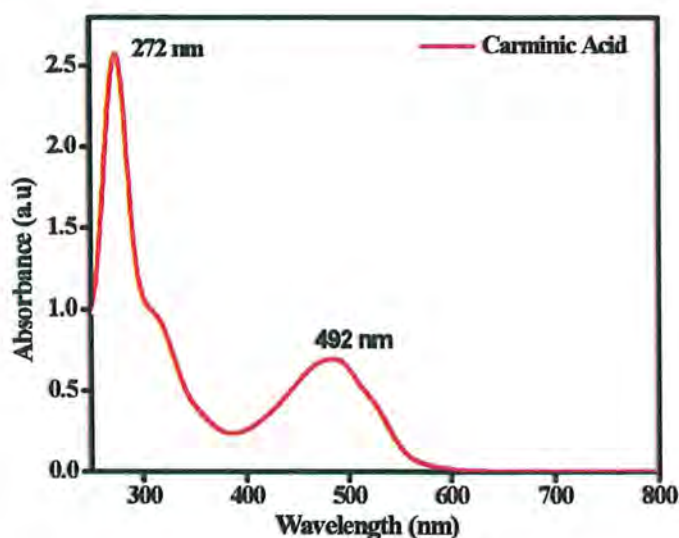
Figure. 3.10. UV-Visible spectrum of CA dye.

3.2.2 UV-Visible Spectrum of Arsenazo III dye

In UV-Visible spectrum of arsenazo III dye two major peaks were observed one at 534 nm and the other at 312 nm. The peak at 534 nm is because of n-π*transitions while the other at 312 nm corresponds to π- π* transitions. The UV-Visible spectrum of arsenazo III is shown below in Figure 3.9.
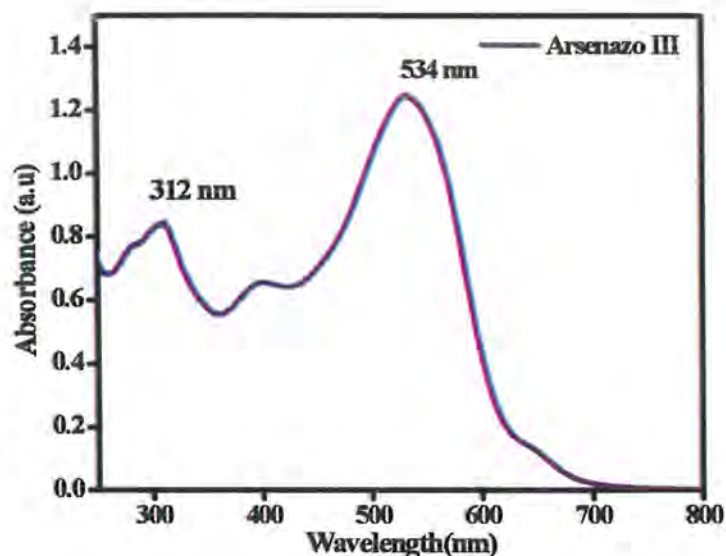
Figure. 3.11. UV-Visible spectrum of AZ dye.

3.3 Optical Properties of Carminic Acid Dye Sensitized Nanoparticles
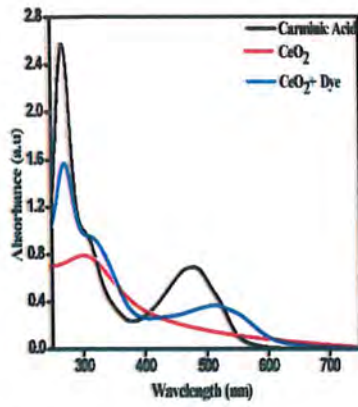
Nanohybrid assemblies were successfully synthesized by the chemisorption of carminic acid dye on the surface of nanoparticles. 1 mM solution of dye was prepared in deionized water and was used as a stock solution. This solution was then used to make different dilutions of dye solution with various concentrations ranging from 25-70 mM. Then concentration of dye was optimized and then that dye solution was then used for chemisorption of dye on the surface of nanoparticles and then UV-Visible spectroscopy was performed to confirm the synthesis of nanohybrid assembly.

These UV-Visible spectra were then compared with UV-Visible spectrum of pure dye and UV-Visible spectrum of nanomaterial. Grafting of pure and different percentages of zirconium doped ceria nanoparticles with carminic acid dye are shown below. The spectrum in black is for the dye while the other one in red is for the nanoparticles.

Carminic acid dye works efficiently in DSSCs because of its wide absorption in ultraviolet and visible region. From the results of UV-Visible spectroscopy it is confirmed that nanohybrid materials were synthesized successfully, there is a wide shift in UV-Visible plot compared to the pure dye in visible region the shift in the broad band of dye in nanohybrid assembly is in the ranges from 492 -560 nm.

41
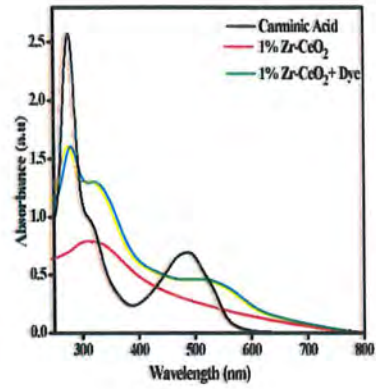
Figure. 3.12. UV-Visible spectra of CA dye grafted with (a) CeO_2 (b) 1% Zr-CeO_2 (c) 2 % Zr-CeO_2 (d) 3% Zr-CeO_2 (e) 4%Zr-CeO_2 (f) 5% Zr-CeO_2

3.4 Optical Study of Arsenazo III Dye Sensitized Nanoparticles (Nanohybrid Materials)

Nanohybrid assemblies were synthesized successfully by the chemisorption of arsenazo III dye on the surface of pure and doped ceria nanoparticles .1 mM solution 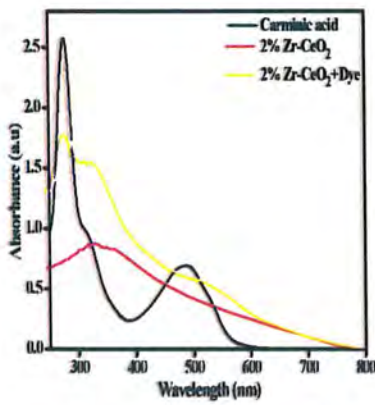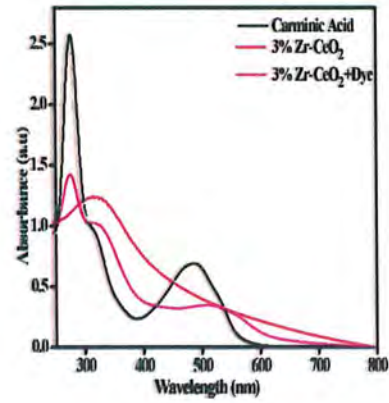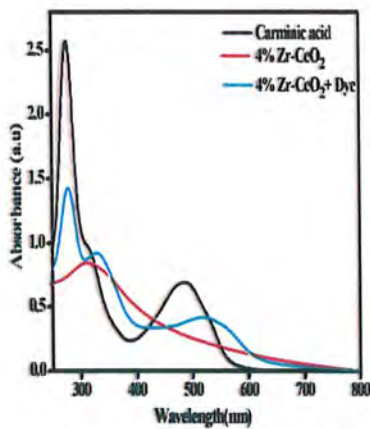of dye was prepared which was then used as a stock solution to prepare the dye solutions of different concentrations ranging from 25-75 mM The concentration of dye solution was then optimized in this case the optimized concentration of the dye used was 50 mM and then it was used for the chemisorption of arsenazo III dye on the surface of pure and doped ceria nanoparticles. The UV-Visible spectroscopy was then carried out to confirm the successful synthesis of nanohybrid assemblies. The UV-Visible spectra of nanohybrid assemblies for arsenazo III sensitized CeO_2 and zirconium doped CeO_2 nanoparticles, these spectra include the UV-Visible spectrum of pure arsenazo III dye, UV-Visible spectrum of nanoparticles and the UV-Visible spectrum of grafted nanoparticles. By comparing the spectrum of pure and grafted material it is clearly seen that nanohybrid assemblies are successfully synthesized. A significant change in the UV-Visible spectrum of grafted sample was observed. A prominent red shift was observed on overlapping the absorption spectrum of grafted samples with the absorption spectrum of pure dye. The broad peak of pure dye was shifted from 534- 590 nm after grafting of dye on the surface of nanoparticles which increases the absorption in visible region and increases the efficiency of DSSCs.
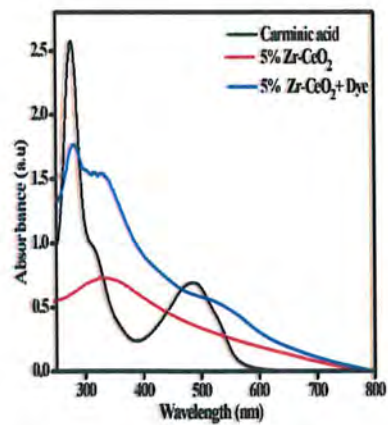
(a)

(b)

(c)
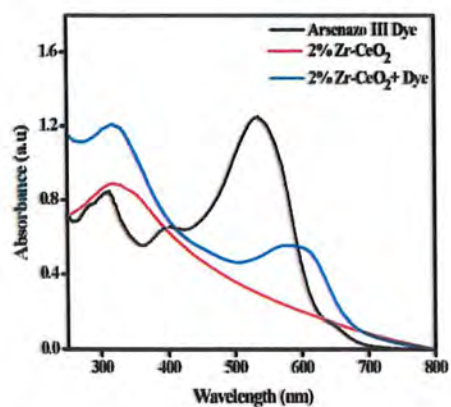
(d)
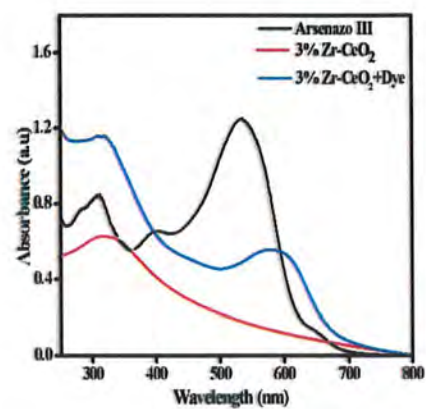
(e)
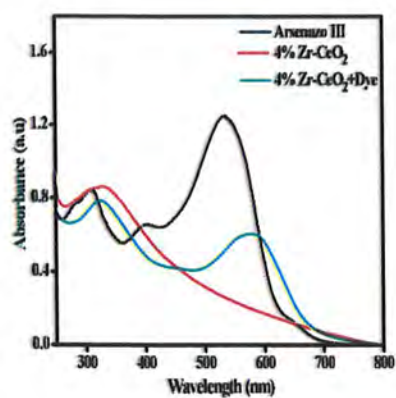
(f)
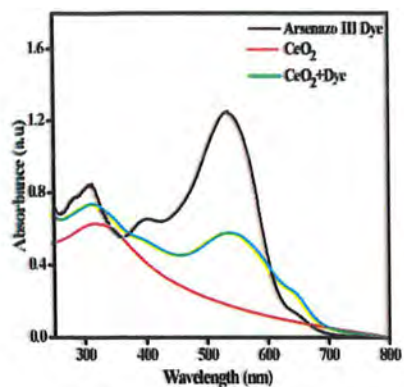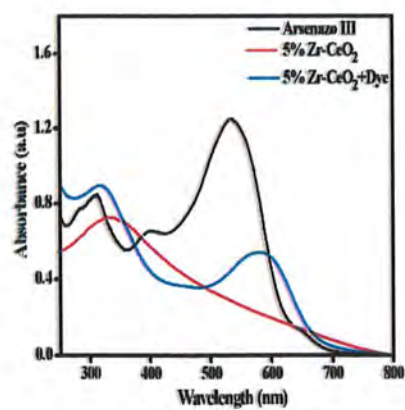

Figure. 3.13. UV-Visible spectra of AZ dye grafted with (a) CeO2 (b) 1% Zr-CeO2 (c) 2% Zr-CeO2 (d) 3% Zr-CeO2 (e) 4%Zr-CeO2 (f) 5% Zr-CeO2
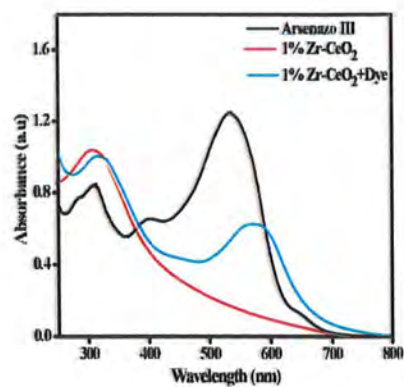
3.5 FT-IR Analysis of Pure Dye and Nanohybrid Material

3.5.1 FT-IR Analysis of Carminic Acid Dye

FT-IR is the technique to reveal the impurities in the material and tells us about the sample purity. Its spectrum distinguishes the functional groups in the compound by showing their characteristic peaks. FT-IR spectrum of carminic acid dye is shown in the Figure 3.12.
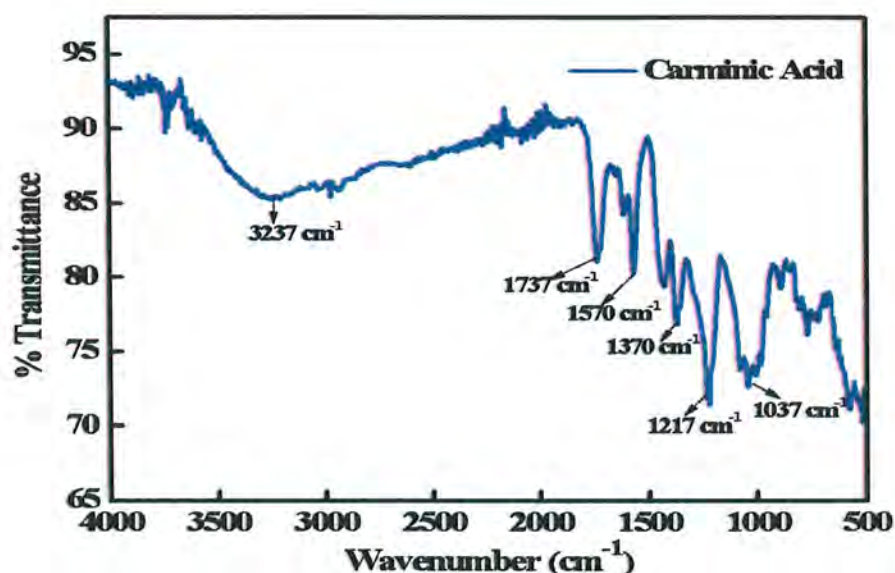
Figure. 3.14. FT-IR spectrum of CA dye.

The appearance of the broad band at 3237 cm^{-1} in the FTIR spectrum of the dye corresponds to the O-H starching frequency. The band at 1737 cm^{-1} verified the starching vibrations of acidic functionality in carminic acid dye. Stretching vibrations of C-C, C=OH vibrations, and C-H vibrations were responsible to allot peaks from 1000 to 1500 cm^{-1}.

3.5.2 FT-IR Analysis of Nanoparticles Grafted with Carminic Acid Dye

FT-IR spectrum of nanohybrid is shown in the Figure 3.13, by comparing the FT-IR spectrum of nanohybrid material and the pure dye, it is verified that that the nanohybrid assemblies are successfully synthesized because certain peaks of dye molecule are absent in the grafted dye samples. This is confirmed by comparing the FT-IR spectrum of pure carminic acid dye and that of the grafted samples. Figure 3.13

45

is comparing the FT-IR spectrum of carminic acid dye with the pure ceria nanoparticles with the dye molecule adsorbed on the surface.
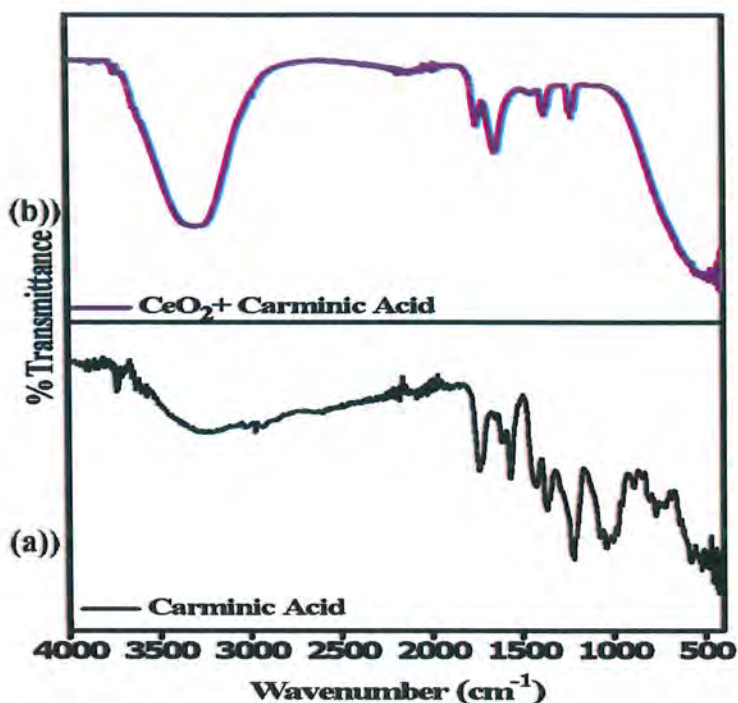
Figure. 3.15. Comparing the FT-IR spectrum of (a) CA dye with (b) CA grafted pure ceria nanoparticles.

While the Figure 3.14 is showing the FT-IR spectra of dye molecule grafted onthe surface of ceria nanoparticles doped with different percentages of zirconium.
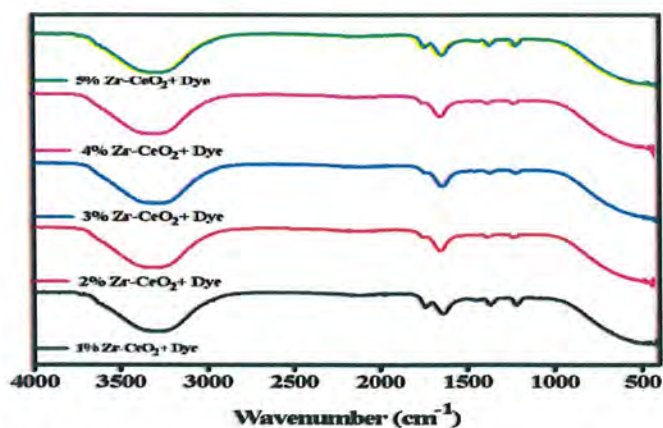
Figure. 3.16. FT-IR spectra of ceria nanoparticles doped with (1-5)% zirconium.

3.5.3 FTIR Analysis of Arsenazo III Dye

Arsenazo III is an azo dye, used here as a photosensitizer in DSSC. FT-IR spectrum of

the arsenazo III dye is shown in Figure 3.17. FT-IR spectrum of amolecule not only reveals the major functional groups present in the molecule but also its purity. FT-IR spectrum of dye molecule exhibits a broad band at 3444 cm^{-1} which corresponds to the starching vibrations of O-H bond present in the molecule. The peakat 2758 cm^{-1} is due to starching of phenyl C-H bond, while peaks at 2359 cm^{-1}, 1569 cm^{-1} and 1488 cm^{-1} are due to the CO2 absorption, S=O stretching and phenyl N=N stretching. Peak at 762 cm^{-1} is due to =O asymmetric vibration while peak at 622 cm^{-1}is because of As-OH symmetric stretch.
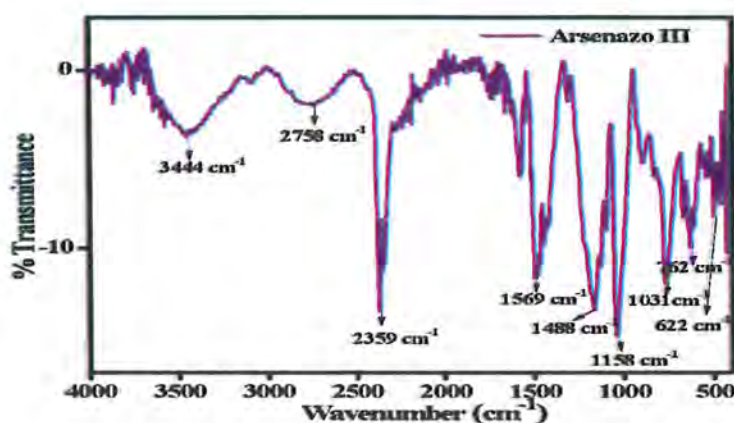
Figure. 3.17. FT-IR spectrum of the AZ dye.

3.5.4 FT-IR Analysis of Nanoparticles Grafted with Arsenazo III Dye

FT-IR spectra of dye sensitized pure CeO$_2$ and zirconium doped CeO$_2$ are given. Confirmation for the successful synthesis of nanohybrid assembly using arsenazo III dye and nanoparticles was obtained by analyzing the FT-IR spectra of pure dye and the grafted nanoparticles. Most of the peaks present in the FT-IRspectrum of dye molecule indicating presence of the acidic anchoring groups are absent in case of grafted samples, which showed that chemisorption of dye on the surface of nanoparticles is successfully achieved. Figure 3.16 is comparing the FT-IR spectrum of pure arsenazo III dye and the FT-IR of arsenazo III dye adsorbed on the surface of pure CeO$_2$ nanoparticles. While Figure 3.17 shows FT-IR spectra of graftedceria nanoparticles doped with different percentages of zirconium.
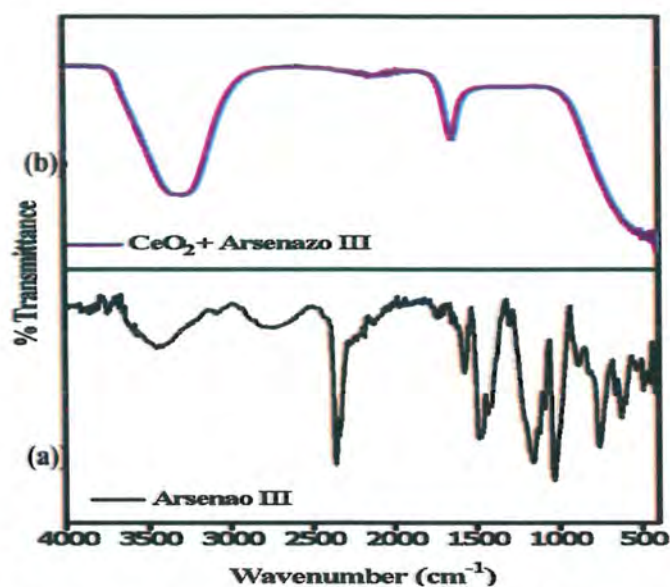
Figure. 3.18. Comparing the FT-IR spectrum of (a) AZ dye with (b) AZ grafted pure ceriananoparticles.
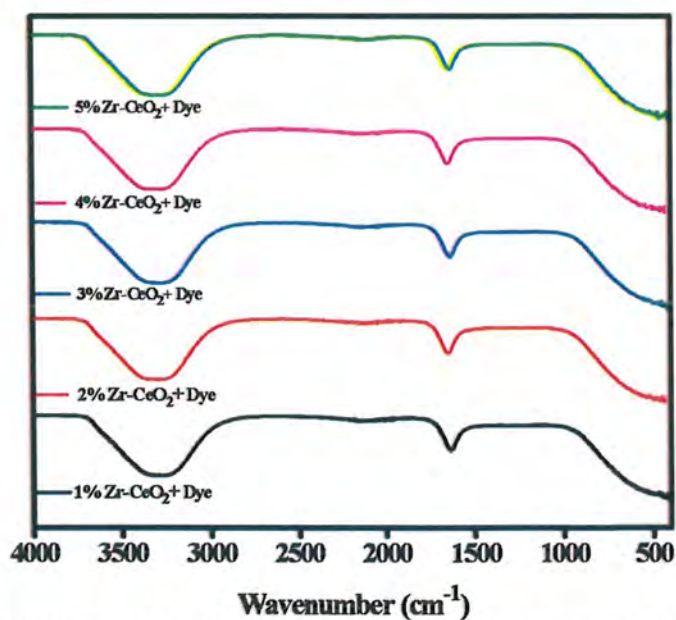
Figure. 3.19. FT-IR spectra of AZ dye grafted ceria nanoparticles doped with and (1-5)%zirconium.

3.6 Current Voltage Measurements (I-V Measurements)

With hole transport material Poly 3-hexylthiophene (P3HT) along with the dye loaded porous nanoparticles of CeO_2 in DSSCs, the efficiency of the cell was calculated. This study explored the use of P3HT as hole conducting material alongside CeO_2 loaded with carminic acid and arsenazo dye and their efficiency tested in dye-sensitized solar cells. Figure 3.19 represents the current voltage plots of DSSCs while the table showing the characteristic photovoltaic parameters.
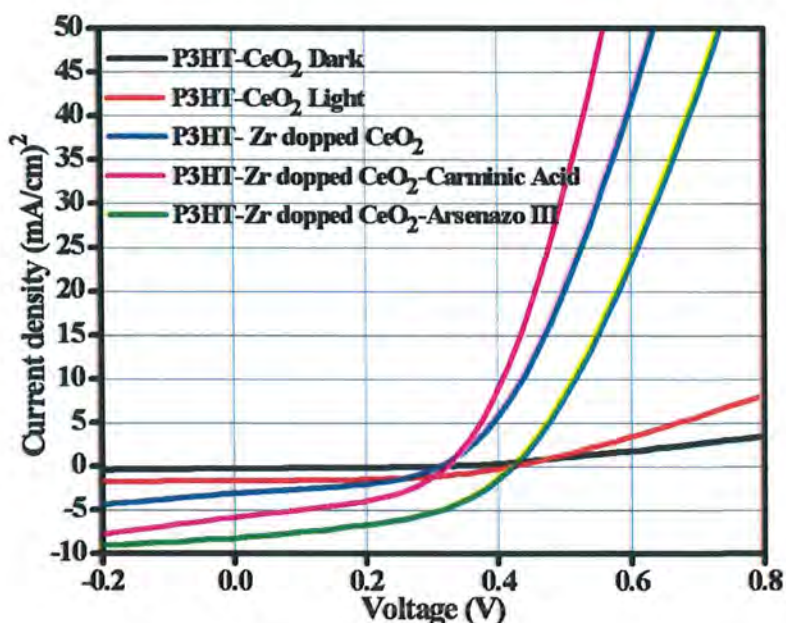
Figure. 3.20. Current-voltage plots of DSSCs.

The open circuit potential (V_{oc}), short circuit current (J_{sc}), maximum power point (M_{pp}), fill factor (**FF**), along with the efficiency of each cell (**η%**) is shown in the table. DSSC with porous zirconium doped ceria nanoparticles loaded with the arsenazo III dye showed the maximum efficiency and had shown to possess the potential characteristic parameters than those of other cells fabricated for this study.

The solar cell with Zr-CeO_2-Arsenazo III resulted in 1.58% efficiency with J_{sc} **of 8.2** mA/cm^2 which is highest among all the cells fabricated, this increase in short circuit current is because of increased light absorption and the generation of increased numbers of charge carriers.

Table 3.3: Evaluation of open circuit potential (V_{oc}), short circuit current (J_{sc}), maximum power point (M_{pp}), fill factor (**FF**) along with the efficiency (**η%**) of each cell.

Cell Composition	J_{sc} (mA/cm^2)	V_{oc} (mV)	M_{pp} (mW/cm^2)	FF	η%
P3HT- CeO$_2$ Light	0.99	0.43	0.18	0.45	0.18
P3HT- Zr doped-CeO$_2$	3.12	0.31	0.40	0.41	0.40
P3HT- Zr dopped CeO$_2$ -Carminic Acid	5.83	0.33	0.81	0.42	0.81
P3HT- Zr dopped CeO$_2$ -Arsenazo III	8.24	0.43	1.58	0.45	1.58

Conclusions

Pristine CeO_2 and (1-6)% transition metal (Zr) doped CeO_2 NPs were successfully synthesized by co-precipitation method. The synthesized nanoparticles were characterized by using UV-Visible spectroscopy, XRD, and FT-IR analysis. UV-Visible spectroscopy indicated that with an increase in zirconium percentage ranging from 1 to 5%, an increase in the wavelength (304-339 nm) was observed and with a further increase in dopant percentage, a blue shift was observed. Tauc plots were used to find out band gaps of the synthesized nanoparticles which showed tuningin the band gap ranging from 3.25 to 2.65 eV. XRD calculations showed that the average crystallite size decreases with an increasing percentage of zirconium (11.5- 7.1nm). There was no impurity peak or Zr-related phases were found in XRD patterns. FT-IR analysis showed the absence of any impurity and also showed the vibration bands of the required samples. Nanoparticles were successfully grafted with carminic acid and arsenazo III dye. Successful fabrication of nanohybrid assemblies wereconfirmed by UV-Visible and FT-IR spectroscopy. Cost effective DSSCs were fabricated using the synthesized nanohybrid using P3HT as a hole transport material. From the I-V plots it was found that Arsenazo III dye sensitized zirconium doped CeO_2 and Carminic Acid dye sensitized zirconium doped CeO_2 resulted in increased efficiency of the cell. It is evident from power conversion efficiency that zirconium doped cerium oxide nanoparticles grafted with carminic acid and arsenazo III dye are effective junctions for photocurrent generation in DSSCs with the efficiency of 0.81 and 1.58 respectively. Arsenazo III dye sensitized zirconium doped CeO_2 nanoparticles showed the maximum efficiency compared to there reference cell.

REFERENCES

1. Bella, F.; Sacco, A.; Pugliese, D.; Laurenti, M.; Bianco, S., Additives and salts for dye-sensitized solar cells electrolytes: what is the best choice? *J. Power Sources* **2014**, *264*, 333-343.

2. Jun, E.; Kim, W.; Chang, S. H., The analysis of security cost for different energy sources. *Appl. Energy* **2009**, *86*, 1894-1901.

3. Tahvonen, O.; Salo, S., Economic growth and transitions between renewable and nonrenewable energy resources. *Eur. Econ. Rev.* **2001**, *45*, 1379-1398.

4. Soudi, N.; Nanayakkara, S.; Jahed, N. M.; Naahidi, S., Rise of nature-inspired solar photovoltaic energy convertors. *Sol. Energy* **2020**, *208*, 31-45.

5. Liu, J.; Cao, G.; Yang, Z.; Wang, D.; Dubois, D.; Zhou, X.; Graff, G. L.; Pederson, L. R.; Zhang, J. G., Oriented nanostructures for energy conversion and storage. *ChemSusChem* **2008**, *1*, 676-697.

6. Li, L.; Gibson, E. A.; Qin, P.; Boschloo, G.; Gorlov, M.; Hagfeldt, A.; Sun, L., Double-layered NiO photocathodes for p-type DSSCs with record IPCE. *Adv. Mater.* **2010**, *22*, 1759-1762.

7. Buchberg, H.; Lalude, O.; Edwards, D., Performance characteristics of rectangular honeycomb solar-thermal converters. *Sol. Energy* **1971**, *13*, 193-221.

8. Drouvelis, P.; Schmelcher, P.; Diakonos, F., Global view on the electronic properties of two-electron anisotropic quantum dots. *Phys. Rev. B* **2004**, *69*, 35333-35341.

9. Gu, L.; Srot, V.; Sigle, W.; Koch, C.; van Aken, P.; Scholz, F.; Thapa, S. B.; Kirchner, C.; Jetter, M.; Rühle, M., Band-gap measurements of direct and indirect semiconductors using monochromated electrons. *Phys. Rev. B* **2007**, *75*, 195214-195220.

10. Nakade, S.; Kanzaki, T.; Kubo, W.; Kitamura, T.; Wada, Y.; Yanagida, S., Role of electrolytes on charge recombination in dye-sensitized TiO_2 solar cell (1): the case of solar cells using the I-/I$_3$-redox couple. *J. Phys. Chem. B* **2005**, *109*, 3480-3487.

11. Sah, C.-T.; Noyce, R. N.; Shockley, W., Carrier generation and recombination in pn junctions and pn junction characteristics. *Proc. IRE* **1957**, *45*, 1228-1243.

12. Kerr, M. J.; Cuevas, A., General parameterization of Auger recombination in crystalline silicon. *J. Appl. Phys.* **2002**, *91*, 2473-2480.

13. Luque, A.; Martí, A.; Antolín, E.; Tablero, C., Intermediate bands versus levels in non-radiative recombination. *Physica B* **2006**, *382*, 320-327.

14. O'regan, B.; Grätzel, M., A low-cost, high-efficiency solar cell based on dye-sensitized colloidal TiO2 films. *Nature* **1991**, *353*, 737-740.

15. Nazeeruddin, M. K.; Kay, A.; Rodicio, I.; Humphry-Baker, R.; Müller, E.; Liska, P.; Vlachopoulos, N.; Grätzel, M., Conversion of light to electricity by cis-X2bis (2,2'-bipyridyl-4, 4'-dicarboxylate) ruthenium (II) charge-transfer sensitizers (X= Cl⁻, Br⁻, I⁻, CN⁻, and SCN⁻) on nanocrystalline titanium dioxide electrodes. *J. Am. Chem. Soc.* **1993**, *115*, 6382-6390.

16. Grätzel, M., Conversion of sunlight to electric power by nanocrystalline dye-sensitized solar cells. *J. Photochem. Photobiol.* **2004**, *164*, 3-14.

17. Arjunan, a. T.; Senthil, T., Dye sensitised solar cells. *Mater. Technol.* **2013**, *28*, 9-14.

18. Bejerano, T.; Gileadi, E., Formation of Thick Layers of Iodine During the Anodic Oxidation of Iodide on a RDE: II. Open-Circuit Behavior. *J. Electrochem. Soc.* **1977**, *124*, 1720-1732.

19. Matthews, D.; Infelta, P.; Grätzel, M., Calculation of the photocurrent-potential characteristic for regenerative, sensitized semiconductor electrodes. *Sol. Energy Mater. Sol. Cells* **1996**, *44*, 119-155.

20. Kubo, W.; Murakoshi, K.; Kitamura, T.; Wada, Y.; Hanabusa, K.; Shirai, H.; Yanagida, S., Fabrication of quasi-solid-state dye-sensitized TiO₂ solar cells using low molecular weight gelators. *Green Chem. Lett. Rev.* **1998**, *27*, 1241-1242.

21. Karim, N. A.; Mehmood, U.; Zahid, H. F.; Asif, T., Nanostructured photoanode and counter electrode materials for efficient Dye-Sensitized Solar Cells (DSSCs). *Sol. Energy* **2019**, *185*, 165-188.

22. Ooyama, Y.; Harima, Y., Photophysical and electrochemical properties, and molecular structures of organic dyes for dye-sensitized solar cells. *ChemPhysChem* **2012**, *13*, 4032-4080.

23. Ikeda, N.; Koganezawa, T.; Kajiya, D.; Saitow, K., Performance of Si/PEDOT: PSS hybrid solar cell controlled by PEDOT: PSS film nanostructure. *J. Phys. Chem. C* **2016**, *120*, 19043-19048.

24. Li, B.; Wang, L.; Kang, B.; Wang, P.; Qiu, Y., Review of recent progress in solid-state dye-sensitized solar cells. *Sol. Energy Mater. Sol. Cells* **2006**, *90*, 549-573.

25. Savvin, S. B., Analytical use of arsenazo III: determination of thorium, zirconium, uranium and rare earth elements. *Talanta* **1961**, *8*, 673-685.

26. Rowatt, E.; Williams, R. J. P., The interaction of cations with the dye arsenazo III. *Biochem. J.* **1989**, *259*, 295-298.

27. Nogueira, A. F.; De Paoli, M. A.; Montanari, I.; Monkhouse, R.; Nelson, J.; Durrant, J. R., Electron transfer dynamics in dye sensitized nanocrystalline solar cells using a polymer electrolyte. *J. Phys. Chem. B* **2001**, *105*, 7517-7524.

28. (a) Huang, S.; Schlichthörl, G.; Nozik, A.; Grätzel, M.; Frank, A., Charge recombination in dye-sensitized nanocrystalline TiO_2 solar cells. *J. Phys. Chem. B* **1997**, *101*, 2576-2582; (b) Park, N. G.; Van de Lagemaat, J.; Frank; A. J., Comparison of dye-sensitized rutile-and anatase-based TiO_2 solar cells. *J. Phys. Chem. B* **2000**, *104*, 8989-8994.

29. Alharbi, F. H.; Kais, S., Theoretical limits of photovoltaics efficiency and possible improvements by intuitive approaches learned from photosynthesis and quantum coherence. *Renew. Sust. Energ. Rev.* **2015**, *43*, 1073-1089.

30. Baxter, J. B.; Aydil, E. S., Nanowire-based dye-sensitized solar cells. *Appl. Phys. Lett.* **2005**, *86*, 53114-53120.

31. Thomas, S.; Deepak, T. G.; Anjusree, G. S.; Arun, T. A.; Nair, S. V.; Nair, A. S., A review on counter electrode materials in dye-sensitized solar cells. *J. Mater. Chem. A.* **2014**, *2*, 1-15.

32. Ma, T.; Fang, X.; Akiyama, M.; Inoue, K.; Noma, H.; Abe, E., Properties of several types of novel counter electrodes for dye-sensitized solar cells. *J. Electroanal. Chem.* **2004**, *574*, 77-83.

33. Gong, J.; Sumathy, K.; Qiao, Q.; Zhou, Z., Review on dye-sensitized solar cells (DSSCs): Advanced techniques and research trends. *Renew. Sust. Energ. Rev.* **2017**, *68*, 234-246

34. Zhang, Q.; Chou, T. P.; Russo, B.; Jenekhe, S. A.; Cao, G., Aggregation of ZnO nanocrystallites for high conversion efficiency in dye-sensitized solar cells. *Angew. Chem.* **2008**, *120*, 2436-2440.

35. Khanna, P.; Kaur, A.; Goyal, D., Algae-based metallic nanoparticles: Synthesis, characterization and applications. *J. Microbiol. Methods Methods* **2019**, *163*, 105656-105661.

36. (a) Lee, Y. J.; Kim, T. G.; Sung, Y. M., Lattice distortion and luminescence of CdSe/ZnSe nanocrystals. *Nat. Nanotechnol.* **2006**, *17*, 1-12; (b) Reiss, P.; Bleuse,

J.; Pron, A., Highly luminescent CdSe/ZnSe core/shell nanocrystals of low size dispersion. *Nano. Lett.* **2002,** *2,* 1-15.

37. Yang, X.; Wang, L., Synthesis of novel hexagon SnO_2 nanosheets in ethanol/water solution by hydrothermal process. *Mater. Lett.* **2007,** *61,* 3705-3707.

38. Kwon, H.; Park, D. H.; Park, Y.; Silvain, J. F.; Kawasaki, A.; Park, Y., Spark plasma sintering behavior of pure aluminum depending on various sintering temperatures. *Met. Mater. Int.* **2010,** *16,* 71-75.

39. Okuyama, K.; Lenggoro, I. W., Preparation of nanoparticles via spray route. *Chem. Eng. Sci.* **2003,** *58,* 537-547.

40. Hicks, E. M.; Zou, S.; Schatz, G. C.; Spears, K. G.; Van Duyne, R. P.; Gunnarsson, L.; Käll, M., Controlling plasmon line shapes through diffractive coupling in linear arrays of cylindrical nanoparticles fabricated by electron beam lithography. *Nano. Lett.* **2005,** *5,* 1065-1070.

41. Shojaei, M.; Shokuhfar, A.; Zolriasatein, A., Synthesis and characterization of $CuAlS_2$ nanoparticles by mechanical milling. *Mater. Today Commun.* **2021,** *27,* 1-23.

42. Moosa, A.; Ridha, A. M.; Allawi, M. H., Green synthesis of silver nanoparticles using spent tea leaves extract with atomic force microscopy. *Int. J. Curr. Eng.* **2015,** *5,* 3233-3241.

43. Swihart, M. T., Vapor-phase synthesis of nanoparticles. *Colloids Interface Sci. Commun.* **2003,** *8,* 127-133.

44. Asanithi, P.; Chaiyakun, S.; Limsuwan, P., Growth of silver nanoparticles by DC magnetron sputtering. *J. Nanomater.* **2012,** *4,* 1-12

45. Parashar, M.; Shukla, V. K.; Singh, R., Metal oxides nanoparticles via sol–gel method: a review on synthesis, characterization and applications. *J. Mater. Sci.: Mater. Electron.* **2020,** *31,* 3729-3749.

46. Swihart, M. T., Vapor-phase synthesis of nanoparticles. *Curr. Opin. Colloid Interface Sci. 8,* **2003,** 127-133.

47. Swihart, M. T., Vapor-phase synthesis of nanoparticles. *Curr. Opin. Colloid Interface Sci. 8,* **2003,** 127-133.

48. Lu, S.; Liang, J.; Long, H.; Li, H.; Zhou, X.; He, Z.; Zhang, H., Crystal phase control of gold nanomaterials by wet-chemical synthesis. *Acc. Chem. Res.* **2020,** *53,* 2106-2118.

49. Guzmán, M. G.; Dille, J.; Godet, S., Synthesis of silver nanoparticles by chemical reduction method and their antibacterial activity. *Int. J. Chem. Biomol. Eng.* **2009,** *2*(3), 104-111.

50. Dou, X.; Sabba, D.; Mathews, N.; Wong, L. H.; Lam, Y. M.; Mhaisalkar, S., Hydrothermal synthesis of high electron mobility Zn-doped SnO2 nanoflowers as photoanode material for efficient dye-sensitized solar cells. *Chem. Mater.* **2011,** *23*, 3938-3945.

51. Adeeyinwo, C. E.; Okorie, N. N.; & Idowu, G. O., Basic calibration of UV/visiblespectrophotometer. *Int. j. sci. technol* **2013,** *23*, 247-251.

52. Suzuki, Y.; Hino, H.; Hawai, T.; Saito, K.; Kotsugi, M.; & Ono, K., Symmetry prediction and knowledge discovery from X-ray diffraction patterns using aninterpretable machine learning approach. *Scientific reports,* **2020,** *10*(1), 21790.

53. Hinson-Smith, J. P. S. A. V. Product Review: The Endearing FTIR Spectrophotometer, **2003.**

54. Kumar, D. K.; Kříž, J.; Bennett, N.; Chen, B.; Upadhayaya, H.; Reddy, K. R.; Sadhu, V., Functionalized metal oxide nanoparticles for efficient dye-sensitized solar cells (DSSCs): A review. *Mater. Sci. Energy Technol.* **2020,** *3*, 472-481.

55. Hegazy, A.; Kinadjian, N.; Sadeghimakki, B.; Sivoththaman, S.; Allam, N. K.; Prouzet, E., TiO2 nanoparticles optimized for photoanodes tested in large area Dye-sensitized solar cells (DSSC). *Sol. Energy Mater. Sol. Cells* **2016,** *153*, 108-116.

56. Mahmoud, S. A.; Fouad, O. A., Synthesis and application of zinc/tin oxide nanostructures in photocatalysis and dye sensitized solar cells. *Sol. Energy Mater. Sol. Cells* **2015,** *136*, 38-43.

57. Zhang, J.; Gao, L., (2004). Synthesis and characterization of antimony-doped tin oxide (ATO) nanoparticles by a new hydrothermal method. *Materials chemistry and physics,* **2004,** *87*, 10-13.

58. Sowmya, N.; Bykkam, S.; V Rao, K., Synthesis and characterization of ceria-titania (CeO2-TiO2) core-shell nanoparticles for enzymatic bio sensing application. *Curr. Nanomater.* **2016,** *1*, 132-138.

59. Bharathi, R. N.; Sankar, S., Structural, optical, and magnetic

properties of Nd-doped CeO_2 nanoparticles codoped with transition metal elements (Cu, Zn, Cr). *J. Supercond. Nov. Magn.* **2016**, *31*, 2603-2615.